POLITECNICO DI TORINO

MASTER'S THESIS

Single-Trial Analysis of Readiness Potentials using Empirical Mode Decomposition

Candidate:
Simone RUMAC

Supervisors:
Professor Gabriella Olmo
Professor Vito De Feo

Corso di laurea in Ingegneria Biomedica

September 13, 2018


POLITECNICO DI TORINO
1859
1906

POLITECNICO DI TORINO

Abstract

Facoltà di Ingegneria Biomedica
Politecnico Di Torino

Master of Science

Single-Trial Analysis of Readiness Potentials using Empirical Mode Decomposition

by Simone RUMAC

Since discovery of the slow negative electroencephalographic (EEG) activity preceding self-initiated movement by Kornhuber and Deecke, many studies arose to investigate the relationship between this signal, called Readiness Potential or *Bereitschaftspotential*, and free will; in the early 80's, Benjamin Libet designed an experiment that allowed him to demonstrate that the intention to perform a movement begins about half a second before the actual movement is initiated. Therefore, if it were possible to narrowly detect the presence of intention, we could gain important information about the state of consciousness of patients that present the locked-in syndrome (LIS) and ultimately it could be useful to discriminate between these patients and patients in a vegetative state.
In order to do so, the present thesis work proposes a general framework for the analysis of movement intention from the EEG signal; specifically, we meant to retrieve the Readiness Potential both from the average over many trials and from a single trial recording. Given the very low signal-to-noise ratio, single-trial analysis represents a challenging task: in this work, we present a detector, based on the Empirical Mode Decomposition (EMD) framework coupled with spatial and Savitzky-Golay filters, that allowed for a better characterization of the RP, and resulted in significant noise reduction.

Contents

List of Figures

List of Tables

Chapter 1

Introduction

1.1 The Central Nervous System (CNS)

The central nervous system is the responsible organ for everything we perceive, do, feel, think and sense; it gives to each one of us its personality and the active consciousness of our personal identity. It also coordinates the activity of all the other organs, and is fundamental in the maintaining of the homoeostases.

1.1.1 Anatomy of the Central Nervous System

The CNS consists of the encephalon (or brain) and the spinal chord. Because of its jelly-like tissue, it is a very vulnerable part of our body: therefore, it is protected by glial cells, bones, connective tissue and fluid.

Glial Cells

When we think about the nervous system, we think of neurons; nonetheless, about 75-90% of the CNS is made by the glial cells, which not only serve a supporting function to the neurons, but also play an active role in the communication between them. Many studies showed that the glial cells have an important role in some neurodegenerative diseases, like multiple sclerosis, Alzheimer's disease and Parkinson's disease.
There are five types of glial cells: oligodendrocytes, astrocytes, ependymal cells, Schwann cells and microglia.
Glial cells have multiple physiological functions: astrocytes are the most differentiated glial cells: they are, for instance, involved in the normal development of a special kind of capillaries that limit the movements of some molecules between the blood and the CNS, forming a system known as blood-brain barrier. To a lesser degree, oligodendrocytes and Schwann cells contribute also to the normal development of the nervous system.
Astrocytes guide the neurons development to their correct destination, and control the development and maintaining of synapses. They support axon regeneration and have a key role in the maintaining of the normal extracellular environment that surrounds the neurons, and especially the synapses.
In particular, they maintain the correct level of potassium outside the synapses, and remove some neurotransmitters; moreover, they synthesize and store

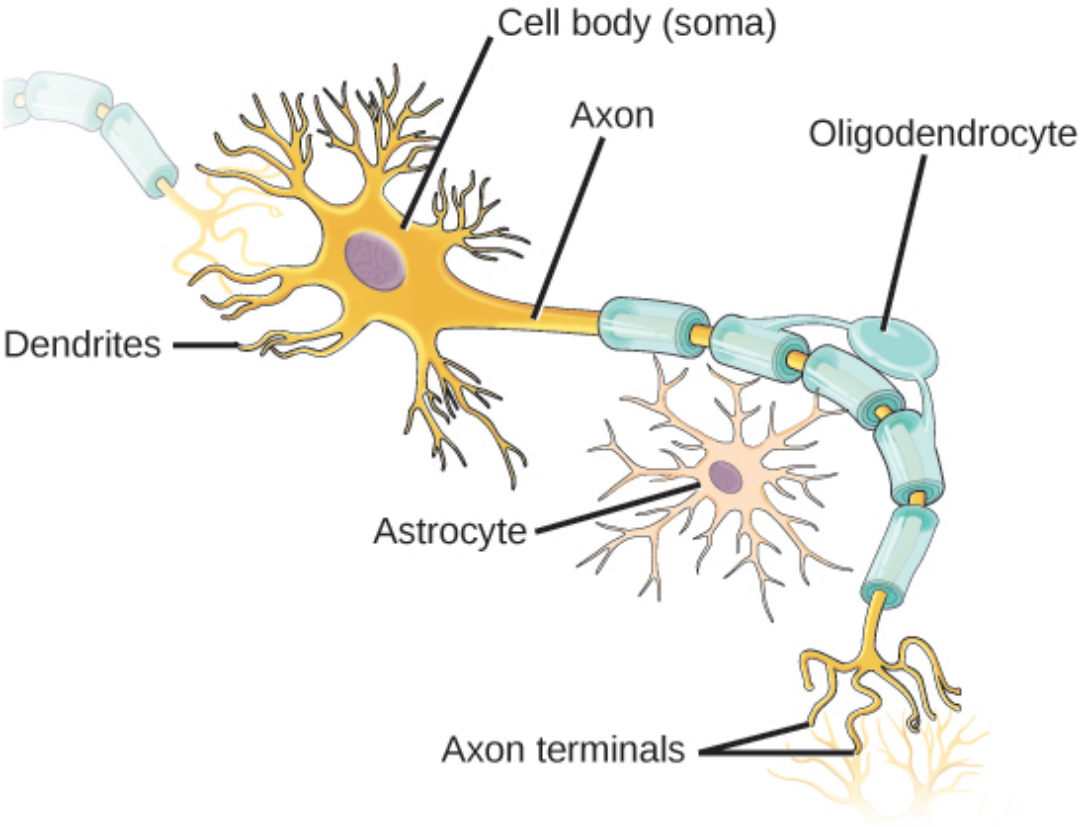

FIGURE 1.1: The principal cellular components of the CNS. By CNX OpenStax , via Wikimedia Commons.

substances (like glycogen) that will be later used by the neurons. Astrocytes and microglia both have a protective function from toxic substances.

Cerebrospinal fluid (CSF)

The cerebrospinal fluid is a clear liquid that wets the CNS; it has a very similar composition to plasma, albeit not identical. The cerebrospinal fluid not only surrounds the CNS, but infiltrates it as well, surrounding neurons and glial cells, and filling some cavities that are present in the brain and spinal chord.
The encephalon contains four of these cavities, called ventricles, that communicate between each other. The total amount of CSF is varies from 125 to 150 ml; it covers numerous functions, like protecting the delicate nervous tissue from impacts.
Moreover, it contributes to keep constant the ionic composition outside the cells, which is a key factor to the correct excitability of tissues. Like the extracellular fluid, it provides the correct nutrients to glial cells and neurons, and removes waste products.

Blood-Brain Barrier

In most tissues, glucose, oxygen and other substances can diffuse through the capillaries, the thinnest blood vessels of our body; small molecules like gasses, non-organic ions, monosaccharides and amino acids can all freely penetrate the walls of the capillaries. While hydrophobic molecules pass through the plasmatic membranes, hydrophilic molecules pass through pores that are present in-between endothelial cells. Bigger molecules, however, cannot move with this system: in the majority of tissues, they are exchanged in a process known as transcytosis - the movement of one molecule from one cell to another via endocytosis followed by esocytosis.
In the CNS, many hydrophobic molecules pass trough the endothelial cells of the capillaries, but transcytosis does not happen, and the exchange of hydrophilic molecules between the CNS cells is limited by the blood-brain barrier. This physical barrier between the blood and the cerebrospinal fluid protects the brain from toxic substances that can be present in the blood: hydrophilic substances that must be actively passed through the endothelial membrane by mediated transport - like sugars and amino acids - do not penetrate the blood-brain barrier, because of the high selectivity of the specific carriers of the brain cells.
Therefore, the brain is only selectively penetrable, which makes it more resilient to infections, but also harder to reach with pharmaceutical drugs.

White and Grey Matter

The Central Nervous System presents a highly ordered structure; the cellular bodies, the dendrites, the axons end-plates create structures known as *clusters*, that macroscopically appear of grey colour. The axons are also grouped together, but, on the other hand, appear white. Therefore, we talk of grey (about 40% of the brain) and white (the remaining 60%) matter .
Looking at the whole brain structure from outside, it appears grey: this is due to the fact that it is almost entirely covered by a thin layer of grey matter, called Cerebral Cortex. The white matter resides inside the brain, with the exception of some small areas of grey matter, known as *nuclei*, that reside in deeper areas. In the spinal chord, this disposition is inverted, with the white matter on the external layer, and the grey matter on the inside.

Cerebral Cortex

The cerebral cortex represents the most recent (in evolutionary terms) area of our brain; it is situated on its most external layer, and consists of a thin layer of grey matter, whose thickness varies between 1.5 mm and 4 mm. On the cerebral cortex, more than a billion of neuron are contained, with up to a thousand billion (10^{12}) of synapses.
The grey matter of the cerebrum is deeply folded to give a convoluted appearance, and can be divided in two hemispheres (left and right), which can

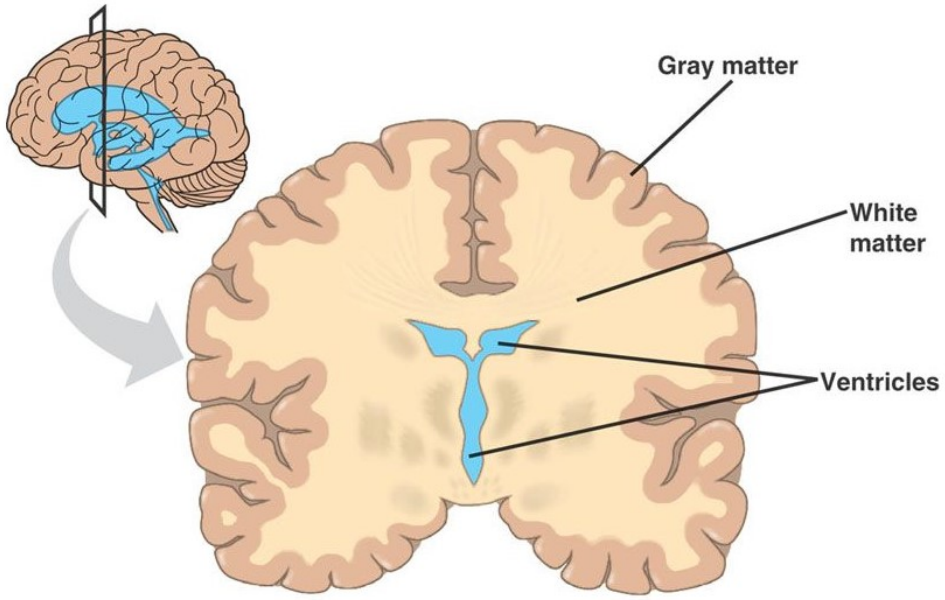

FIGURE 1.2: Grey and White Matter distribution.

be further divided in four regions, known as lobes. Each lobe contains functionally specialized areas, which roughly link to particular tasks performed by the brain.

1. **Frontal Lobe**
   The frontal lobe contains the primary motor cortex, which is of special interest to our work: the Readiness Potential, in fact, demonstrates the involvement of the motor cortex and supplementary motor area in the pre-motor planning of volitional movement; for this reason, as we will see later, the electrodes that pick up the activity of this two particular areas are of primary importance. This area contains also regions that are specialized in speech elaboration and personality determination.

2. **Temporal Lobe**
   The temporal lobe contains the areas that allow us to elaborate the hearing and smelling senses; it is also involved in processing this sensory inputs into derived meanings for the appropriate retention of visual memory, language comprehension, and emotion association.

3. **Parietal Lobe**
   The parietal lobe contains a region known as the somatosensory cortex, which is related to the elaboration of stimuli such as pain, tact, temperature; some areas of the parietal lobe are also important in language processing.

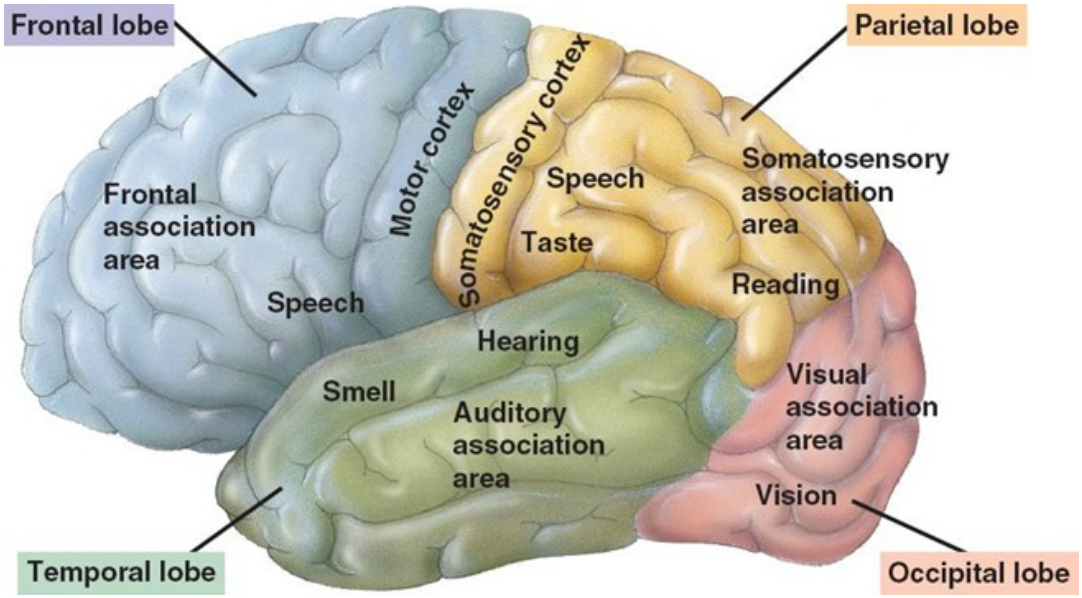

FIGURE 1.3: The Brain Lobes and their main functions.

4. **Occipital Lobe**
   Also known as visual cortex, the occipital lobe is deputed to the elaboration of visual stimuli, visuospatial processing, colour differentiation, and motion perception.

1.2 The EEG Signal

The electroencephalogram is the direct measure of the electrical activity of the brain. Usually, in standard EEG, the electrodes are posed on the scalp, and therefore it is a non-invasive procedure. Invasive EEG (*electrocorticography*) is also possible, but much less common. EEG is most often used to diagnose epilepsy, which causes abnormalities in EEG readings, but can also be used to indicate sleep disorders, measure the depth of anaesthesia or coma, diagnose encephalopathy and brain death.

1.2.1 How the EEG is generated

The electrical activity recorded by the EEG depends on the total sum activity of many different neurons inside the brain. In particular, the electric field generates from the pyramidal neurons located in the third and fifth strata of the cerebral cortex; normally, the visible oscillations of an EEG recording are generated by the post synaptic potentials, which are of very small amplitude (fractions of mV), but last considerably longer than the action potentials: consequently, they are much more likely to create a spatial and temporal sum [19] [18].

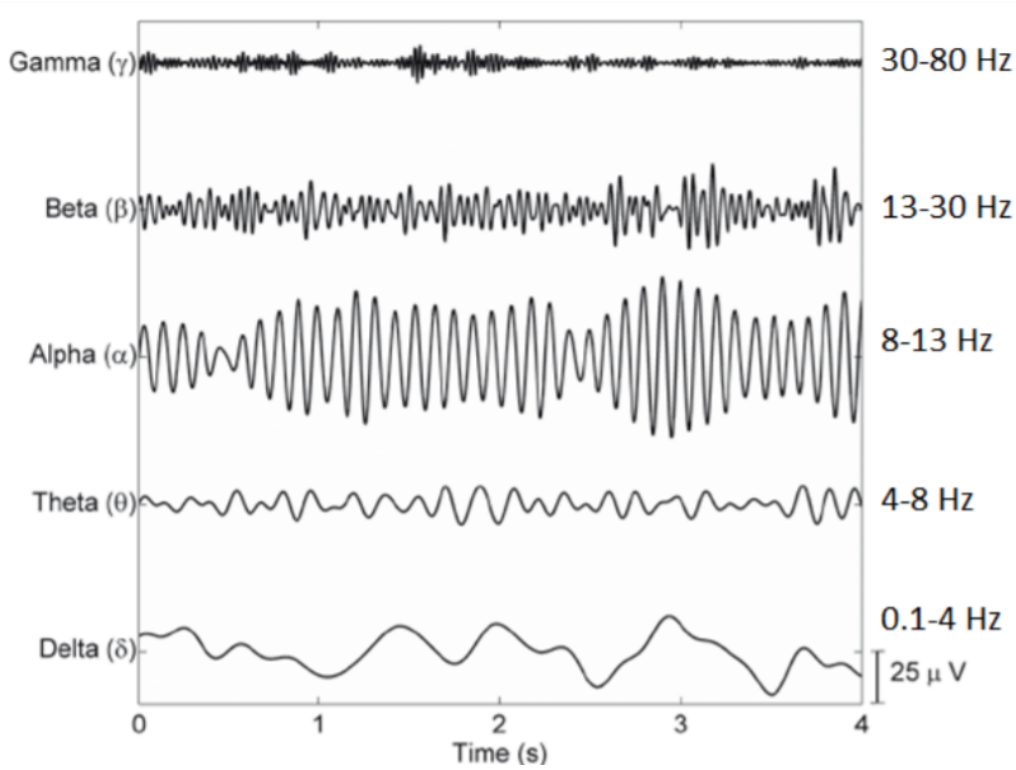

FIGURE 1.4: A graphic representation of the five EEG Rhythms.
Source: K.Blinowska et al., 2012

1.2.2 The EEG Rhythms

As previously said, the EEG reflects the activity of multiple brain regions and cells. For this reason, it is usually difficult to infer from its time representation and many studies focused on its frequency content, which reflects the overall activity of the brain: when many different areas of the brain are activated simultaneously (i.e. the brain is *working*), their synchronization is reduced, and thus, the resulting electric field has higher frequency and lower amplitudes.
It has been observed, mainly during sleep analysis, that the EEG signal presents five typical frequency bands: delta, theta, alpha, beta and gamma waves (plus Mu waves).

1. **Delta (< 4 Hz)**
   Delta waves have the greatest amplitude (75-200 μV) and are usually found during dreamless sleep (third and fourth phase of Slow-Wave Sleep) or in deep meditation states.

2. **Theta (4-7 Hz)**
   Theta rhythms are found during sleep, deep meditation, drowsy and hypnotic states.

3. **Alpha (8-15 Hz)**
   Alpha waves present amplitudes of 30-40 μV, and arise from under the

visual cortex. They are found during wake states with closed eyes, in relaxed environment, or during the moments that precede sleep.

4. **Mu (8-11 Hz)**
   These waves have the same frequency range as the alpha waves, but are mainly found over the motor cortex and depend primarily on its synchronization; therefore, during movement, their amplitude is reduced. This phenomenon is known as Event Related Desynchronization (ERD), and was first investigated by Gert Pfurtscheller in his works [25] [21] [24].

5. **Beta (16-30 Hz)**
   Beta waves appear in states of normal waking consciousness and during task performances. They present low levels of synchronization and amplitude, meaning a state of high cerebral activity.

6. **Gamma (> 30 Hz)**
   Frequency components above 30 Hz are called gamma waves; to this day, their role is still not completely understood, but many have hypothesized that these waves are related to conscious awareness and attentive focus.

1.2.3 Recording the EEG Signal

As previously said, the EEG is obtained by directly measuring the electric potential on the scalp; the first human EEG recording was obtained in 1924 by Hans Berger, using normal radio equipment to amplify the electrical activity on the scalp [30].
Nowadays, the recording system consists mainly of four components: up to 256 electrodes (or electrode cap), the amplification system (with or without analog filters),the A/D converter and the recording device. Since 1958, the International Federation in Electroencephalography and Clinical Neurophysiology adopted a standardized method for electrode positioning, called 10-20 placement system.

1.2.4 The 10-20 Electrode Placement System

The 10-20 International System of Electrode Placement (IS 10-20) is an internationally recognized method to describe the location of scalp electrodes.
The label 10-20 designates the proportional distance in percentages between ears and nose where the points for the electrodes are chosen. Electrode placements are labelled according to the adjacent brain areas: F (frontal), C (central), T (temporal), P (posterior), and O (occipital). The letters are accompanied by odd numbers at the left side of the head, and by even numbers on the right side.
The system is based on the relationship between the location of an electrode and the underlying area of cerebral cortex.

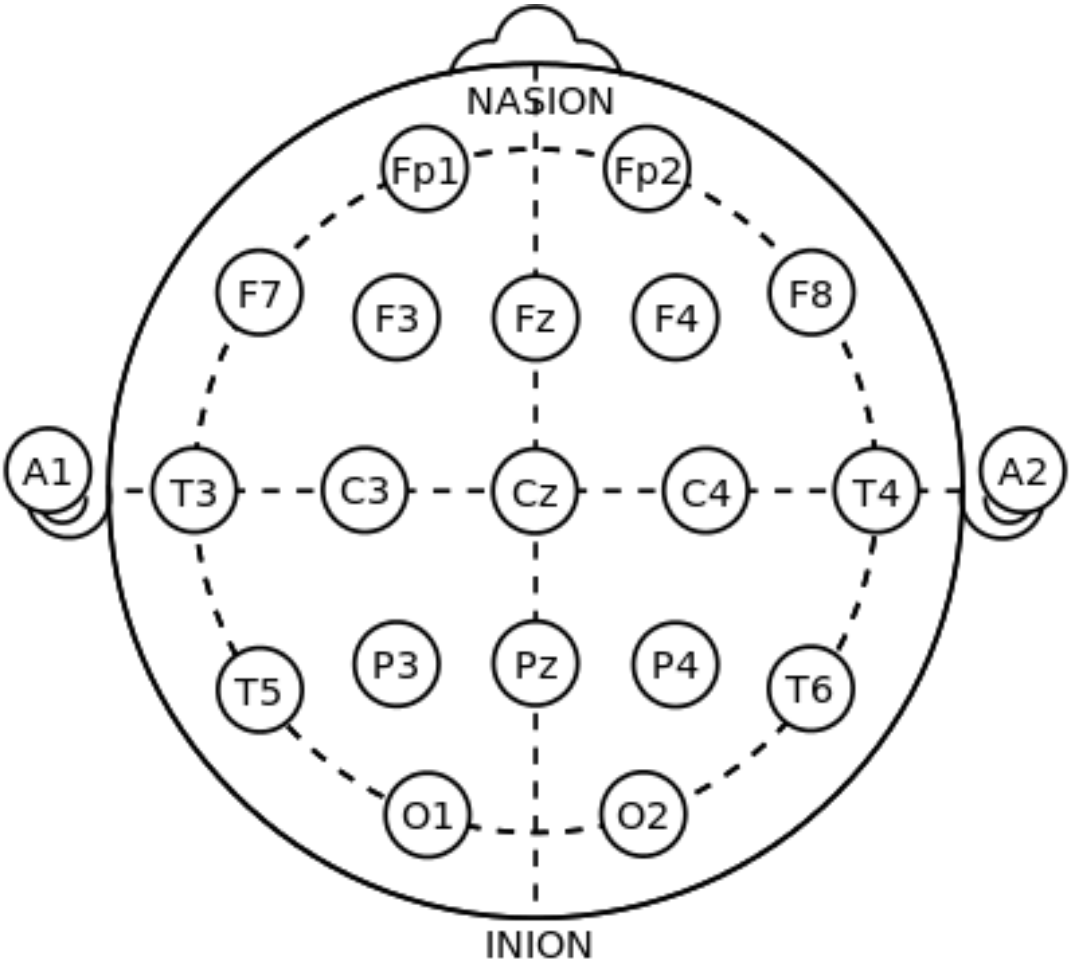

FIGURE 1.5: Electrode placement according to the 10-20 system.

1.2.5 Main Problems of the EEG Recording

The recorded signal amplitudes usually vary from 10 μV to 100 μV, which is fairly close to the order of magnitude of the electrical noise generated from the device. In addition, all external electrical sources may interfere with such a sensitive recording system, making th EEG signal typically very difficult to clean. In this section, we will briefly enumerate the main sources of noise and artefacts present in most recordings.

1. **Power Line Interference**
   This phenomenon is due to the capacitive coupling that occurs between the power line supply and the cables used to extract the signal. The resulting artefact has the form of a sinusoidal wave whose frequency is the same as the AC frequency of the source (i.e. 50 Hz in most countries, 60 Hz in the USA and a handful of others). Usually, this artefact is easy to eliminate using different types of notch filters during the pre-processing phase.

2. **Muscle Movements**
   The electric fields generated by the muscles are usually much stronger than the EEG signal is, and therefore any small movement occurring

during the recording is reflected as an artefact on the signal traces. These artefacts are much more difficult to remove, but usually reside in a frequency band which is of lesser interest, and can be removed by simply low-pass filtering the signal.

3. **Electrode detachment**
   As previously stated, the EEG is a non-invasive procedure: this means that none of its components are inserted inside the subject's body, and thus he or she is not sedated during the recording.
   The electrodes are fixed on the scalp with adhesive materials and the subject can move and breathe during the whole test; these movements can often cause the temporary detachment of some electrodes, with a subsequent increase of the impedance. In these cases, the resulting signal is heavily compromised and the corresponding trials must be discarded.

4. **Ocular Movement Artefact**
   Due to their positioning close to the electrodes, the eyes can interfere with the electrical signal picked up by the EEG electrodes. These artefacts can be quite visible, and to reduce this problem many experimental set-ups record separately the EMG derived from the eye area; during the pre-processing phase, this recorded information is used to reduce the interference, with the aid of various techniques (such as PCA, ICA etc.).

5. **ECG - Pulse, Pacemaker**
   Sometimes, the EEG traces contain spikes that reflect the heart (or pacemaker) electrical activity. This artefact is particularly problematic because of its variability over multiple cardiac cycles.

1.3 Event-Related Potentials (ERP)

Event-related potentials (ERPs) are very small voltages that can be seen in the EEG recording in response to specific stimuli or events. They are thought to be caused by the summed activity of post-synaptic potentials produced when a large number of similarly oriented cortical pyramidal neurons (thousands or millions) are simultaneously activated, while processing information. These EEG changes are time locked to sensory, motor or cognitive events that provide safe and non-invasive approach to study psychological and physiological correlates of mental processes [29].
ERPs in humans can be divided into two categories: the early waves, or components - peaking roughly within the first 100 milliseconds after stimulus - are called 'sensory' or 'exogenous' as they depend largely on the physical parameters of the stimulus. In contrast, ERPs generated in later parts reflect the manner in which the subject evaluates the stimulus and are termed 'cognitive' or 'endogenous' ERPs as they examine information processing.

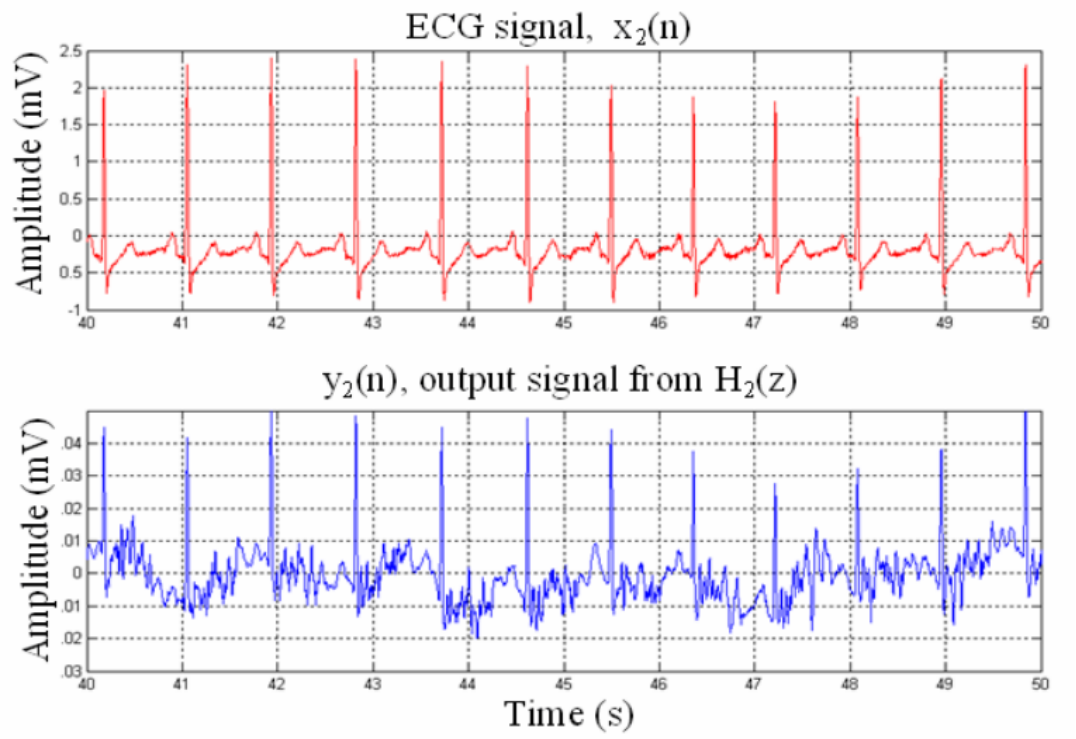

FIGURE 1.6: An example of an EEG simulated signal, corrupted by the ECG and EOG artefacts [8].

Event-related potentials can be elicited by a wide variety of sensory, cognitive or motor events; in the following sections we will focus on some ERPs that are related to movement intention.

1.3.1 Movement-Related Cortical Potentials (MRCP)

MRCPs denote a series of potentials that occur in close temporal relation with movement or movement-like activity. These may occur before, during or after the movement and they refer to movement preparation or intention, localized in the motor cortex.
Kornhuber and Deecke (1965) distinguished four components of the MRCPs: (1) Readiness potential (RP), (2) Reafferent potential, (3) Pre-motion Positivity and (4) Motor Potential. In this work we are mainly interested in the potentials that occur before movement, in particular to the RP, and we may occasionally refer to it as MRCP, LRP or ERP.

1.3.2 The Readiness Potential (RP)

As discussed previously, the EEG signal-to-noise ratio is typically small, and therefore small fluctuations are difficult to see from its temporal representation; the most common method used to improve the SNR is the averaging technique: by computing the average of many epochs relative to one or more time-locked events, the noise component can be significantly reduced, and the underlying variations can be exposed.

In 1964, using this technique, Kornhuber and Deecke discovered a small depolarization in the EEG signal recorded under the motor cortex that preceded movement by 2-1.5 seconds; they called this time-locked event Bereitschaftspotential (BP), or Readiness Potential (RP). Subsequently, the BP has been found to be composed of - at least - two distinct components: around 400 ms prior to the movement onset, the BP shows a significant increase in its gradient: the BP before this change is called 'early BP', while the remaining signal before the onset is called 'late BP'.

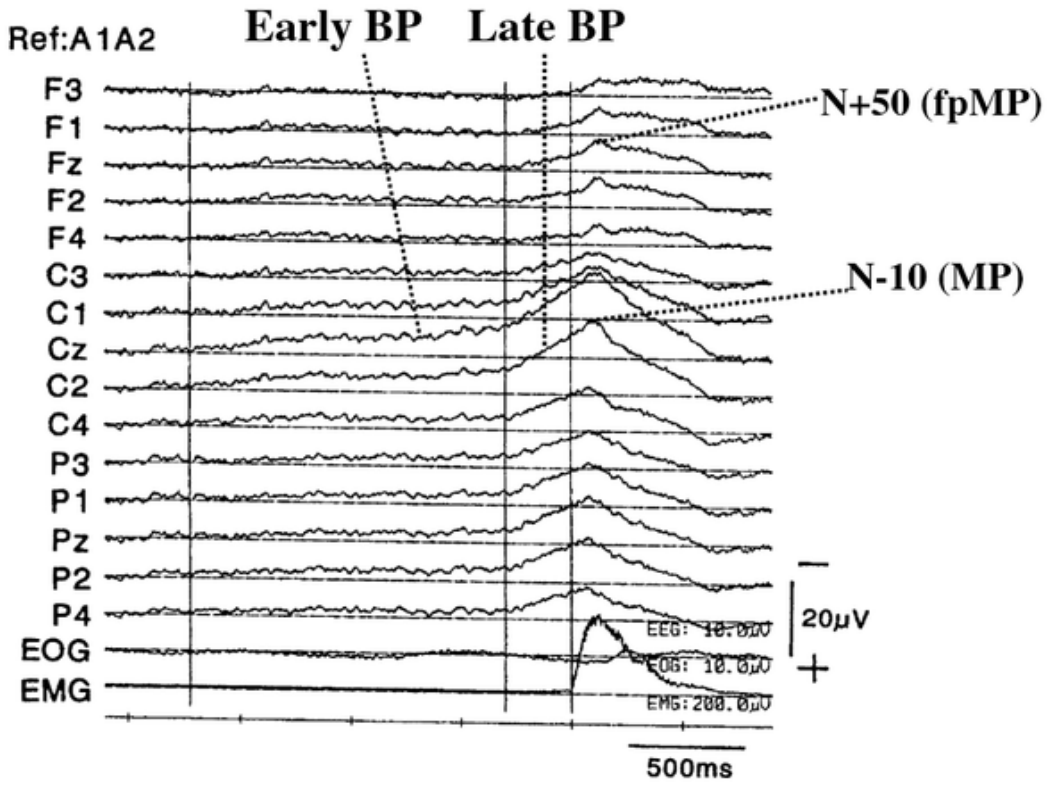

FIGURE 1.7: The averaged BP. [27]

The Lateralized Event-Related Potentials (LRP)

The lateralization of the scalp potential is a phenomenon that concerns the event-related potentials that precede limb movements. The LRP is assumed to be related to selective response activation processes [9].
The Readiness potential is initially equally distributed over both hemispheres, but begins to lateralize before the onset of the muscular response, with larger amplitudes found over the contra-lateral hemisphere.

The Contingent Negative Variation (CNV)

In 2013, P.Ahamadian et al. [26] discovered another similar negative deflection: the Contingent Negative Variation.
In particular, the CNV occurs in specific trials, when the subject is warned

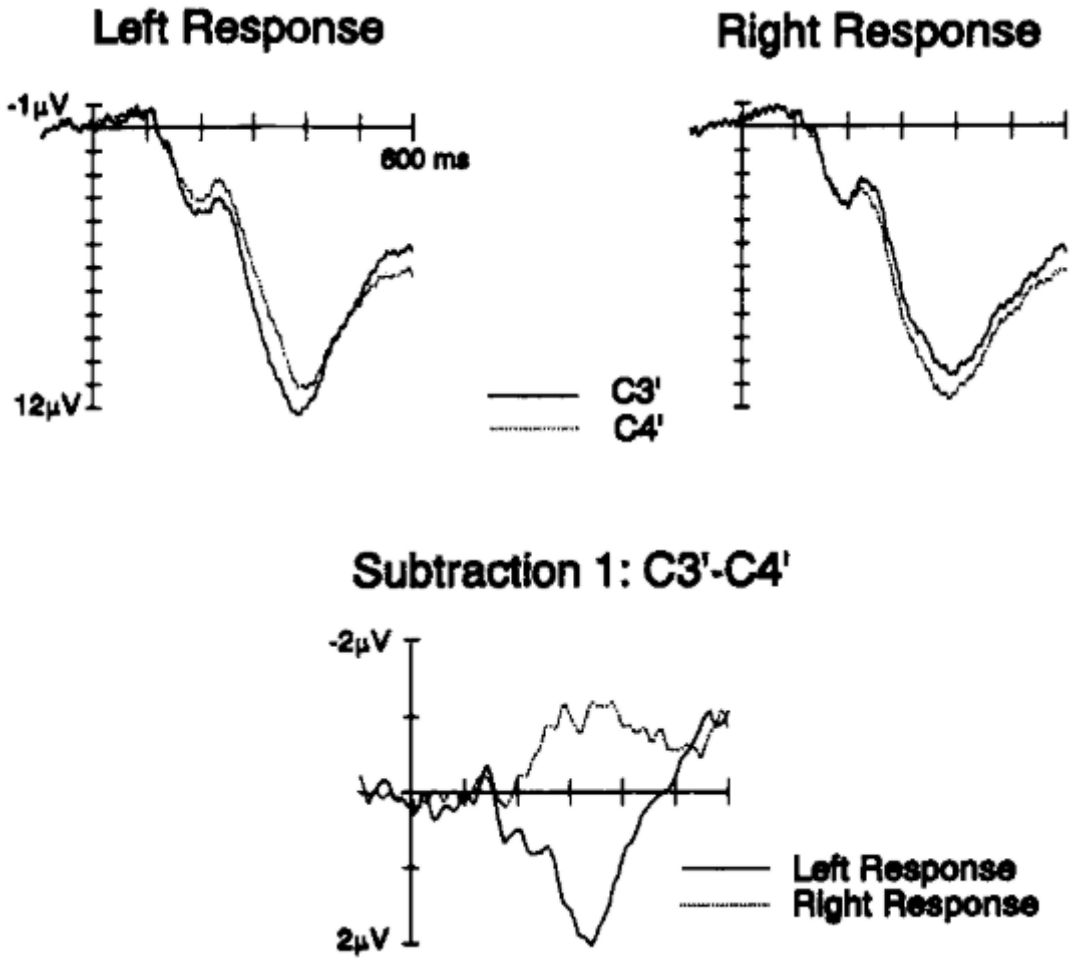

FIGURE 1.8: The lateralized readiness potential, computed with the double subtraction method [9].

by a stimulus that she is going to perform the movement in a short time. Between the warning stimulus and the imperative stimulus, we can observe a slow potential, which becomes lateralized, having larger amplitudes in the contra-lateral hemisphere.

1.3.3 RPs Relationship to Free Will

We stated in previous sections that the readiness potential precedes the actual movement by more than half a second; this discovery lead important scientist to question the relationship between RPs and free will. In particular, one of the first neuroscientists to investigate this field was Benjamin Libet.
In the early 80's, Libet designed an experiment with the aim of answering the question of how does a voluntary act arise in relation to the cerebral processes that mediate it. Ultimately, he was able to demonstrate *"that voluntary acts can be initiated by unconscious cerebral processes before conscious intention appears,*

but that conscious control over the actual motor performance of the acts remains possible" [15].

Libet's Experiment

For his experiment, Libet designed a particular clock using a cathode ray oscilloscope 1.9. The oscilloscope was arranged to have its spot of light revolving near the outer edge of its screen, in order to simulate the sweep of the second hand of a clock. The light dot circled around 25 times faster than a normal 60 seconds clock; thus, each marked second corresponded to about 43 ms.

Subjects were asked to keep looking at the centre of the oscilloscope, at a

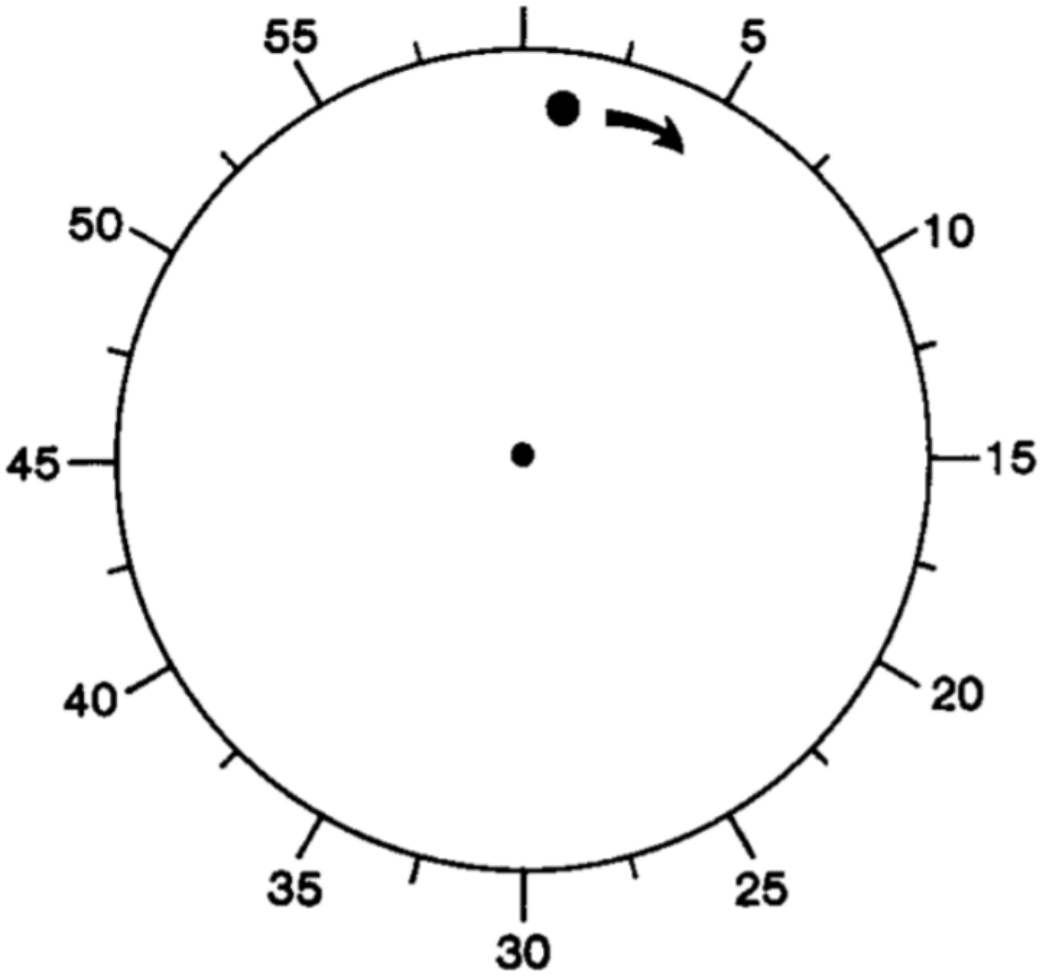

FIGURE 1.9: A schematic representation of the clock used by Libet in his experiment.

distance of about 2.3 meters; then, they were asked to perform a voluntary and not pre-planned flexion of the wrist, at chosen time, and simultaneously take note of the dot position in the moment they were aware of the conscious decision to move.

At the end of 40 trials, the average RP was computed with standard procedure, and compared to the onset of intention as reported by the subject. The first important discovery regarded some series of trials, in which subjects reported to having pre-planned a range of time in which they would have acted (subjects were instructed not to do so). In these cases, the generated ERPs had onsets ranging from 800 ms to 1 second before movement: this lead to the conclusion that, with some constrictions imposed, self-paced movements involved some pre-planning by the subject regarding the instant in which to act. Vice versa, in successful trials, the ERP onsets were found to be around 550 ms before the movement.

On the other hand, the average times reported regarding the intention to act were around the -200 ms mark. This substantial difference - minimum 300 ms - lead to the conclusion that the cerebral initiation of a spontaneous voluntary act begins unconsciously. Put another way, the brain evidently *decides* to initiate or, at the least, prepare to initiate the act at a time before there is any reportable subjective awareness that such a decision has taken place. *However, subjects have reported that some recallable conscious urges to act were 'aborted' or inhibited before any actual movement occurred; in such cases the subject simply waited for another urge to appear which, when consummated, constituted the actual event whose RP was recorded [16].* In this case, free will may manifest itself as a *veto* possibility, that we appear to maintain during the 150 ms or so remaining after the specific conscious intention appears.

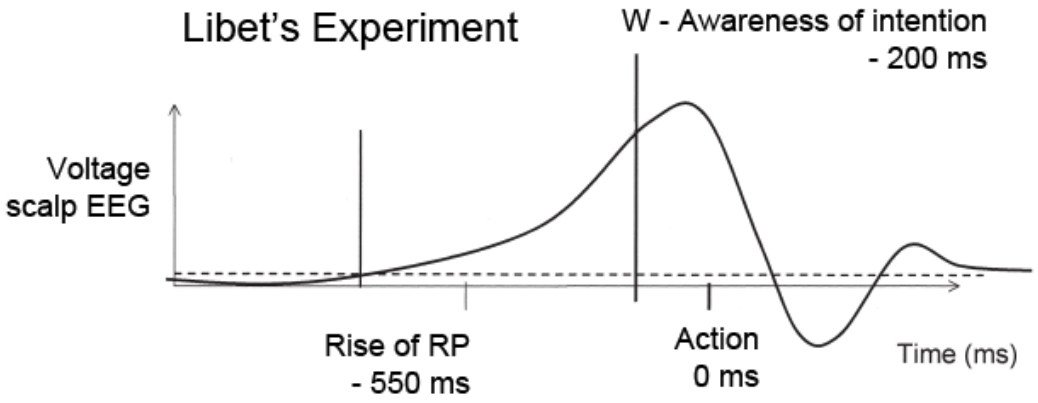

FIGURE 1.10: The time course of a Readiness Potential highlighting the time when the awareness of intention appears. Figure adopted from: `informationphilosopher.com/freedom/libet_experiments.html`

1.4 The Event-Related Desynchronization (ERD)

A number of papers, written between 1975 and 1977 by Gert Pfurtscheller and his group [25] [21] [24], demonstrated for the first time the presence of

an event-related de-synchronization occurring in the alpha band of an EEG recording during sensorimotor stimulation.
This time-locked event, occurring about 2 seconds before the related stimulus (in our case, the onset of a finger movement), can be viewed as a decrease in synchrony of the underlying neuronal populations: on the other hand, when the synchronous activity increases, we have a specular phenomenon called Event-Related Synchronization (ERS), which has also been found in later studies, particularly regarding the last interval of the beta band (26-30 Hz).
In the instantaneous power plot (of a particular frequency band), this synchronization/desynchronization has the form, respectively, of a positive or negative slope: synchronization, in fact, means that the neuronal activity is more likely to add up (in space and time), and therefore the resulting EEG will present higher amplitudes, with consequent increase of its power, and the opposite phenomenon occurs when the activity desynchronizes.
Both ERD and ERS can be explained as generated by changes in one or more parameters that control oscillations in neuronal networks; in particular, they could reflect changes in the activity of local interactions between main neurons and inter-neurons that control the frequency components of the ongoing EEG. [22]

1.4.1 Time course of ERD/ERS

Usually, ERD and ERS phenomena are displayed as a relative variation in power (percentage), with respect to a baseline or reference power level measured before the event. The classic method for its computing, together with another - more recent - one, will be later explained in detail. An averaged time course representation of both phenomena is shown in figure 1.11.

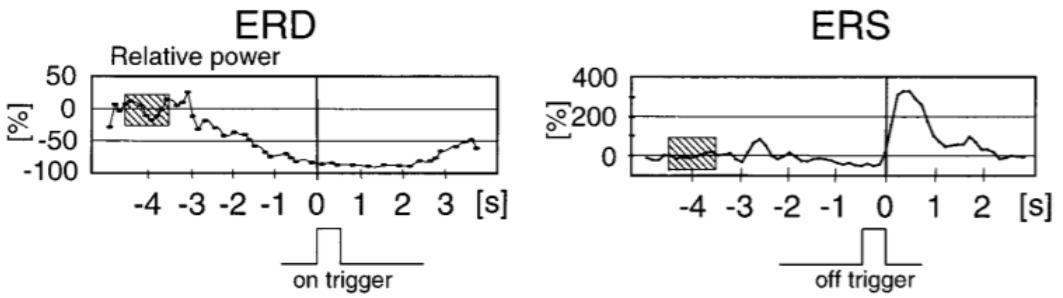

FIGURE 1.11: Averaged plot of ERD and ERS phenomena [22]

1.5 Our Goal

The present thesis work is inserted in a greater research project whose goal is to perform differential diagnosis between two clinical conditions: Vegetative State (VS) and Locked-In Syndrome (LIS).
These two syndromes are very often misdiagnosed, as they present the same

symptoms: VS patients are insensitive to any external stimulus, and differ from comatose patients just because they have their eyes open; patients that present locked-in syndrome, on the other hand, only appear insensitive to any stimulus, but are actually conscious: their non-responsiveness is due to the total paralysis, that includes the eyelids movement and breathing muscles.
Unfortunately, the discrimination between these two conditions is a very difficult task, as the majority of tests rely on a verbal or muscular response from the subject, which is of course impossible in these cases; some studies, like the one performed by Andrews et al. in 1996 [5], reported a misdiagnosis percentage between VS and LIS up to 43%.
Another pertinent clinical condition is called Minimal Consciousness State (MSC), a possible evolution of the coma state. Patients in MSC only show consciousness (intended as self-awareness and awareness of the environment) in response to specific stimuli, and on rare occasions. However, MSC patients cannot communicate reliably with the external environment, as they are unconscious most of the time, and therefore it would be useful to discriminate this clinical condition too.

Ideally, we would hope for a non-invasive and relatively not expensive detection method to discriminate between those conditions. Some patients that have lived a period in LIS condition, and were then able to recover, reported the feeling of wanting to move or speak, but not being able to do so as if body and brain were 'disconnected', in a similar state as what happens during REM sleep. On the contrary, patients in VS condition cannot plan voluntary movements, as they are completely unconscious. For this reason, given that involuntary movements occur in both states, one possible method to perform the correct discrimination would be to detect the *intention* of movement, regardless of the muscular outcome.
In conclusion, the idea of this project is to exploit the Readiness Potential to perform the discrimination, and in particular the first of its components, that seems to be related to movement intention and starts about one second before the actual movement onset.

Chapter 2

Materials

In this chapter we will briefly describe the materials, recording devices and software that were used to perform the analysis. In addition, we will also describe the experimental protocol that was used during the recording phase, on voluntary test subjects.

2.1 Experimental Protocol

All subjects were required to perform three different tasks:

1. the first task was *completely arbitrary*: subjects were instructed to voluntarily - not in a stereotypical way - press a button after an acoustic signal was given; they could perform the movement at any time in a 10 second window after the signal;

2. during the second task subjects were instructed to perform the act in an automatic fashion: this trial was label as *semi-voluntary*;

3. the third task was completely *involuntary*: the EEG signal was recorded after stimulating the patellar tendon with a reflex hammer. During this experiment all subjects were blinded so that they could not see when the stimulus was happening.

Every task was composed of 40 trials. The audio signal was given at random intervals. In this first phase of study, we only considered the completely voluntary movements.

2.1.1 First Dataset Acquisition

The first dataset was acquired during a study about Disorders Of Consciousness at the "Centro Puzzle" of Turin (`centropuzzle.org`), using the Galileo NT instrumentation and its software. For our purposes, we only considered the 15 recordings coming from healthy subjects: 4 males, 11 females, all right-handed, aged between 21 and 26.
The sampling frequency was set to be of 512 Hz, and it was not possible to acquire the electro-oculogram (EOG), usually used in order to improve the removal of artefacts. We used a total of 7 electrodes, placed over the frontal, pre-frontal and parietal cortex: the precise location according to standard 10-20 placement were: : Cz, C3, C4 on the central lobe; Fcz, Fc3, Fc4 on the

frontal lobe; Pz on the parietal lobe and Oz on the occipital lobe.
Ag/AgCl bridge electrodes were used, as long as an EEG electrode fixing belt, with unipolar derivation. The correct electrode placement and impedance was tested using the Galileo NT software package. The same instrumentation was used to obtain the EMG signal: two electrodes were placed on the first phalanx of the right forefinger and on the palm of the hand, at the base of the right thumb.

2.1.2 Second Dataset Acquisition

The second acquisition proceeded using the same parameters, but, instead of using only 7 electrodes, an EEG cap with 64 electrodes was used. The EOG signal was also recorded, which will render eye-artefact removal easier to implement in future analysis.

2.2 Instruments

2.2.1 The GalileoNT

The EEG measurements are acquired using GalileoNT (EEGNT), B8300033000, EBNeuro. During the acquisition, its parameters were set as follows:

- **EEG acquisition**
  - Range: $\pm$ 4 mV;
  - Pass-band filter cut-off frequencies: [50 $\div$ 0.015] Hz;
  - Sampling frequency: 512 Hz;
  - Notch filter: 50 Hz.
- **EMG acquisition**
  - Range: $\pm$ 65 mV;
  - Pass-band filter cut-off frequencies: [500 $\div$ 5] Hz;
  - Sampling frequency: 512 Hz;
  - Notch filter: 50 Hz.

2.3 Software

2.3.1 GalileoNT Software

As briefly stated above, the GalileoNT embedded software allows the user to view the EEG raw data in real-time during the acquisition, to export the EEG file in different formats, to verify the electrode positioning and impedance.

FIGURE 2.1: The GalileoNT Machine.

2.3.2 MATLAB

MATLAB is a fourth-generation programming language and numerical analysis environment.It is used by engineers and scientists in many fields such as image and signal processing, communications, control systems for industry, smart grid design, robotics as well as computational finance.

2.3.3 EEGLAB

EEGLAB is an open-source MATLAB toolbox maintained by the Swartz Centre for Computational Neuroscience (SCCN). This program contains a large number of visualization and processing functions, specifically designed to work with the EEG signal; it also provides an interactive graphic user interface (GUI), allowing users to flexibly and interactively process their high-density EEG and other dynamic brain data using independent component analysis (ICA) and/or time-frequency analysis (TFA), as well as standard averaging methods. We also used the EEGLAB plugin FIRfilt, which allows the user to apply a variety of linear filters to EEGLAB data.

Chapter 3

Methods

The following sections briefly summarize all the methods and algorithms used to perform the analysis. They were divided into three categories, based upon the goal of their implementation regarding our analysis.

3.1 EMG Signal Analysis

Surface electromyogram (EMG) recording is a widely used approach to obtain physiological or clinical information about neuromuscular functions. One its most important applications is the precise detection of motor events; in many cases, such as ours, it is needed to detect the exact onset of a movement. However, due to the stochastic characteristics of the EMG signal, onset detection is a challenging task, especially when the signal to noise ratio (SNR) is very low; in these situations, most common techniques like visual inspection or amplitude threshold are prone to false detections.
To overcome this difficulty, several methods such as double threshold detector, Wavelet template matching or statistical criterion determination have been proposed to improve the performance of onset detection. However, these methods are computationally intense, and a good performance is possible only when a priori knowledge of the processed signal is known.

3.1.1 Teager-Kaiser Energy Operator (TKEO)

In 2006, Xiaoyan et al. from the University of Illinois [14] proposed a simple method to enhance onset detection performances in EMG signals, that exploits the Teager-Kaiser Energy (TKE) non-linear operator.
The discrete TKE operator (Ψ) in time domain is defined as follows:

$$\Psi_d[x(n)] = x^2(n) - x(n+1)x(n-1) \tag{3.1}$$

For a given signal:

$$x(n) = A\cos(\omega_0(n) + \theta) \tag{3.2}$$

where n is the sequence index, ω_0 the angular frequency, A is the amplitude and θ is the initial phase.
We can write:

$$x(n \pm 1) = A\cos[\omega_0(n \pm 1) + \theta] \tag{3.3}$$

and since:

$$\cos(\alpha+\beta)\cos(\alpha-\beta) = \frac{1}{2}[\cos(2\alpha)+\cos(2\beta)] \tag{3.4}$$

$$\cos(2\alpha) = 1-2\sin^2(\alpha) = 2\cos^2(\alpha)-1 \tag{3.5}$$

It follows:

$$x(n+1)x(n-1) = A^2\cos[\omega_0(n-1)+\theta]\cos[\omega_0(n+1)+\theta] \tag{3.6}$$

and ultimately:

$$x(n+1)x(n-1) = x^2(n) - A^2\sin^2(\omega_0 n) \tag{3.7}$$

Therefore, we can write the following relationship:

$$\Psi_d[x(n)] \approx A^2\sin^2[\omega_0(n)] \tag{3.8}$$

3.1.2 EMG onset detection

Regarding the EMG signal, we know that when a motor unit action potential fires, it usually generates an increase in signal amplitude and instantaneous frequency; as we can see from equation 3.8, the output of the TKE operator is proportional to both those parameters (A and ω_0), and we can take advantage of this property to improve the detection system performances: the output will have sharper and narrower spikes corresponding to muscle activity, an it will be easier to implement a thresholding algorithm for onset detection [28].
Usually, the threshold is set to be proportional to the mean of the signal during idle state, plus a multiple (j) of its standard deviation, according to the following equation:

$$threshold = \mu + j\sigma \tag{3.9}$$

with μ as the mean, σ as the standard deviation, and j to be determined. The algorithm is explained in figure 3.1.

3.2 ERD Detection Methods

In the following section, we will give a brief explanation of two methods for the computation of ERD/ERS from an epoched EEG signal. The first one is the classic algorithm used by Pfurtscheller in many of his early publications [24]; the second was chosen from two comparison reviews of many modern methods, one made by Allen et al. [3], the other made by Pfurtscheller in 1999 [22].
Based on these reviews, we choose to implement one of the more promising techniques, which exploits the Continuous Wavelet Transform (CWT).

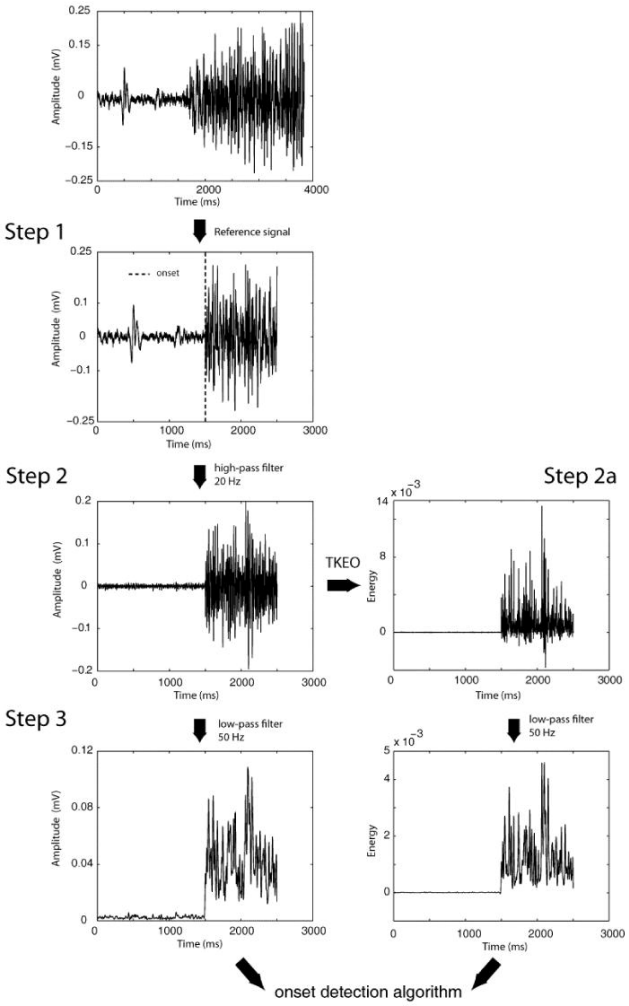

FIGURE 3.1: EMG onset detection using TKE Operator [28].

3.2.1 Band Power Method

The classical method to compute the time course of ERD and ERS includes the following steps:

1. bandpass filtering of all trials;
2. squaring of the amplitude samples to obtain power samples;
3. averaging of power samples across all trials;
4. averaging over time samples to smooth the data and reduce the variability.

As previously specified, the $ERD - ERS$ is then computed as a percentage relative to a reference interval (e.g. 4 to 3 seconds before the movement onset):

$$ERD\% = 100\frac{(A - R)}{R} \tag{3.10}$$

where R is the mean power computed in the reference interval and A is

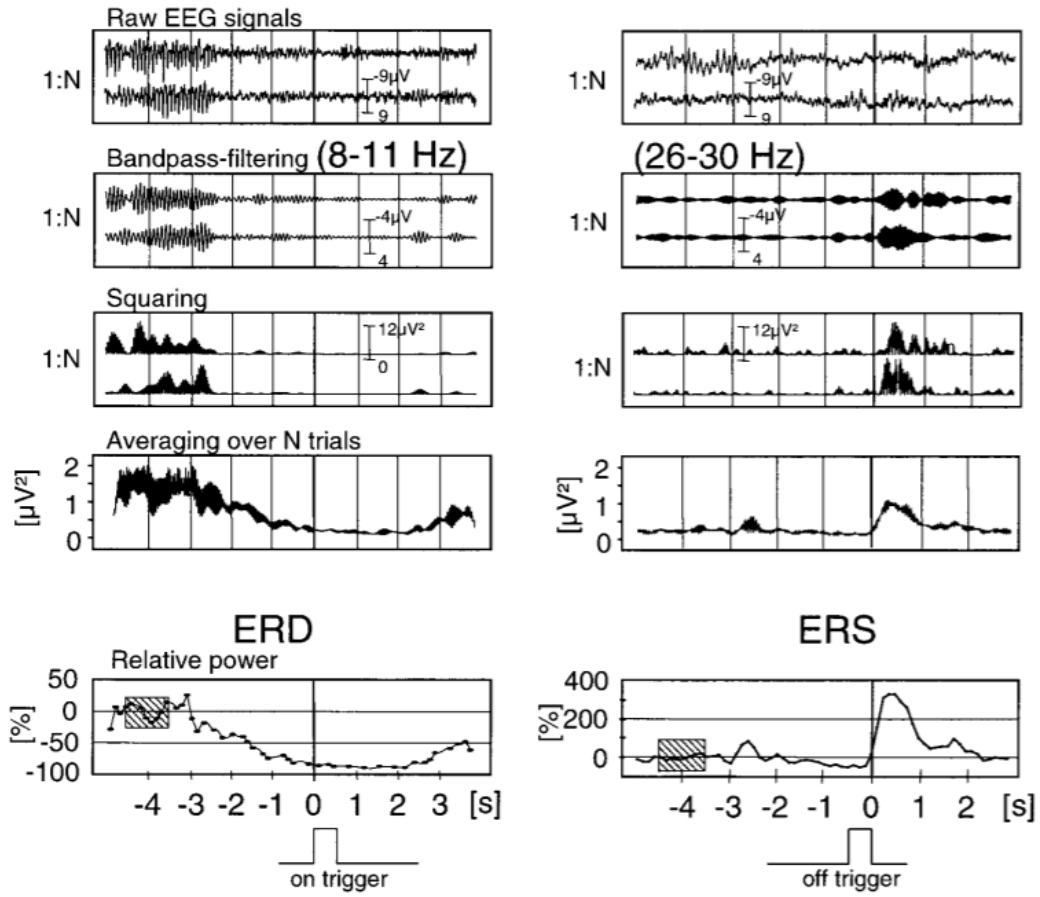

FIGURE 3.2: Averaged plot of ERD and ERS phenomena [22].

the instantaneous power sample. The complete procedure is summarized in figure 3.2.

3.2.2 Continuous Wavelet Method

The Continuous Wavelet Transform (CWT) is a time-frequency representation method used to improve both temporal and spectral resolution compared to standard Short-Time Fourier Transform. This improvement is obtained by expanding the signal of interest onto a set of variable-length basis functions, that are called wavelets.
The mother-wavelet length varies according to the spectral components of the signal, and is no longer fixed as for normal STFT; this technique potentially allows for an improvement of spectral and temporal resolution, as low frequencies are decomposed using longer wavelets, while higher frequency components are analysed using shorter versions of the mother-wavelet, better suited for capturing fast-moving oscillations [3].
The CWT of a signal $x(\tau)$ is defined in equation 3.11 where ψ^* is the complex conjugate of the mother wavelet function and b and a are the translation and scale parameters, respectively.
As we can see, this method computes - for every time sample - the correlation

between the object signal and the wavelet function, delayed by b and scaled by a.

$$CWT_x(a,b) = \frac{1}{\sqrt{a}} \int_{-\infty}^{\infty} x(\tau)\psi^* \left(\frac{\tau - b}{a} \right) d\tau \tag{3.11}$$

After applying the transform, we obtain the energy density of the signal as follows in 3.12:

$$P_\chi(a,b)_{\text{CWT}} = |\text{CWT}_\chi(a,b)|^2 \tag{3.12}$$

3.2.3 The Morlet Transform

By matching the wavelet basis function to the object signal characteristics, we can obtain the wavelet transform which is better suited for its analysis. For *ERD* and *ERS* analysis, the complex Morlet Wavelet has been found to have good performances, due to the oscillatory features of its basis functions [3] [31].
As defined in 3.13, the basis function is equivalent to a complex sinusoid with Gaussian envelope:

$$\psi(t) = \frac{1}{\pi^{1/4}} \exp\left(i2\pi f_0 t\right) \exp\left(-\frac{t^2}{2}\right) \tag{3.13}$$

$$\hat{\Psi}(f) = \pi^{1/4} \sqrt{2 \exp\left(-\frac{1}{2}\left(2\pi f - 2\pi f_0\right)^2\right)} \tag{3.14}$$

In Wavelet Analysis, there is no physical relationship between a and Fourier Frequency, but for the Morlet Transform the central frequency f_0 at each scale can be loosely interpreted as a localised Fourier frequency. This comes from the fact that, if the mother wavelet is localised at a given frequency f_0, then a scaled version $\psi(ax)$ is localised at frequency f_0/a by the scaling property of the Fourier transform [7].
Therefore, we can perform a conversion from time-scale axes of the scalogram to a time-frequency representation: the complex CWT becomes as per 3.15:

$$\text{CWT}_x(t,f) = \sqrt{\frac{f}{f_0}} \int_{-\infty}^{\infty} x(\tau)\psi^* \left(\frac{f(\tau - t)}{f_0} \right) d\tau \tag{3.15}$$

We can then calculate its energy density distribution using 3.12.

3.3 Single-Trial Estimation

In this section, we will briefly describe some of the procedures and techniques used during the single trial analysis. As stated previously, the goal of these methods is to find whether the Readiness Potential is present or not in a single trial recording (i.e., four seconds before and after the movement onset).
To obtain this result, three different techniques have been implemented: first, we applied a Laplacian spatial filter, used to enhance the spatial resolution

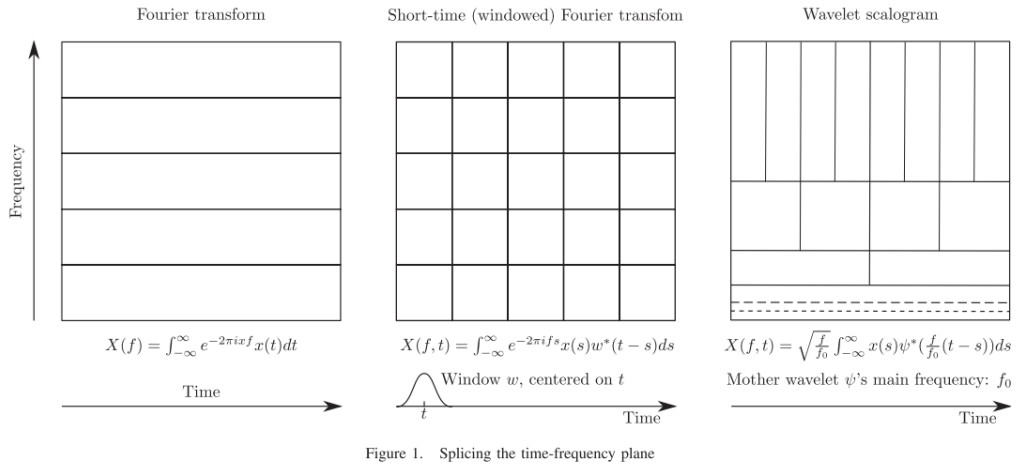

FIGURE 3.3: A graphica representation of the Morlet Wavelet Transform, adapted from [7].

of the signal; secondly, to further improve the SNR, we used the EMD technique and - in cascade - the Savitzky-Golay filtering technique.

3.3.1 Spatial Filtering

Many studies [18] have demonstrated that it is possible to improve the SNR of the EEG signal by implementing a spatial filter; in EEG analysis, four different filters are commonly used, and were compared by McFarland et al. [18] [13] [20] in 1997: Common Average Reference (CAR), large and small Laplacian, and ear reference.
The principle of spatial filtering is quite simple: by combining the signals from different channels, one can either reduce the non-common component (noise reduction), or enhance the common component: in both cases, the results hopefully lead to a better signal-to-noise ratio.

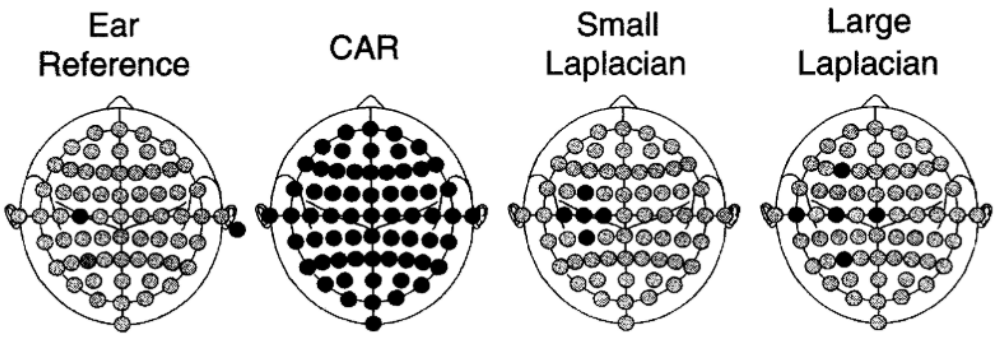

FIGURE 3.4: Geometrical arrangement of four different spatial filters [18].

Large Laplacian Filter

The selected spatial filter was the Large Laplacian (LLSF), which has been proven to be very useful by the above-mentioned papers (among many others). Its very simple implementation follows the subsequent formula, where x_i is the filtered (combined) signal and N_{ch} is the number of channels, which depends on the acquisition system: i refers to the selected central channel, while the other components are shown in figure 3.4.

$$x_i = \begin{cases} 1, & i = 1 \\ -\frac{1}{(N_{\text{ch}}-1)}, & i \neq 1 \end{cases} \tag{3.16}$$

3.3.2 Empirical Mode Decomposition (EMD)

The empirical mode decomposition (EMD) is a signal decomposition method that decomposes non-periodic and non-stationary signals into a finite number of intrinsic mode functions (IMFs).
The original signal $x(t)$ can be re-obtained as the sum of every IMF and a residual. Each IMF must only satisfy two conditions:

1. it must have an equal number of extremes and zero crossings, or differ by no more than one;
2. the mean value of the two envelopes resulting from the interpolation of local maxima and minima is zero at any point [11] [4].

Given an input signal $x(t)$, to perform empirical mode decomposition, the following algorithm must be followed [12]:

1. Find the local extrema of $x(t)$;
2. generate the upper ($e_m(t)$) and lower ($e_l(t)$) envelopes, by interpolating all maxima and minima;
3. compute the local mean as $m_1(t) = \frac{e_l(t)+e_m(t)}{2}$;
4. extract the details $h_1(t) = x(t) - m_1(t)$;
5. verify that $h_1(t)$ satisfies the two conditions mentioned above;
6. if the conditions are not met, repeat 1 to 4 until an IMF is obtained.

When the algorithm converges, we have extracted the first IMF from our signal; we can now repeat this procedure to find the next IMF, by using as a new input signal the residual $r_1 = x(t) - IMF_1(t)$. This can be repeated until the residual signal becomes monotonic, signalling the end of decomposition.

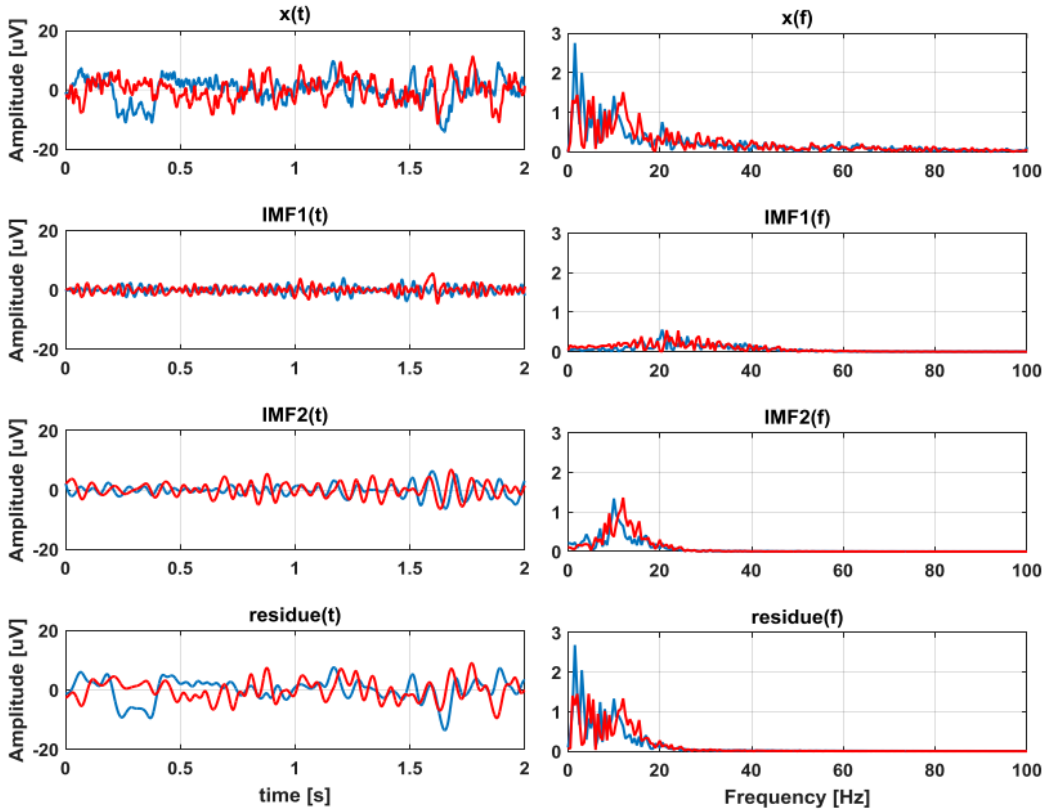

FIGURE 3.5: Example of empirical mode decomposition applied to the EEG signal: the first two IMFs were extracted, and a residue. The red line depicts the basal activity, the blue line is the motor activity (μV) [4].

3.3.3 EMD-Based Signal Denoising

To perform signal de-noising, when the noise component is transient, non-stationary and wide-band, linear methods often do not suffice; to overcome this issue, many non-linear methods like the wavelet-based ones have been developed.
In recent papers [19] [6], Empirical Mode Decomposition has been proposed as part of a non-linear framework to perform denoising in these cases. The major advantage of the EMD is that the basis functions are derived from the signal itself, therefore making the analysis adaptive, in contrast to the wavelet method where the basis functions are predetermined [19].
To perform denoising using the EMD technique, the recovered IMF can be filtered before reconstruction with methods such as the Savitzky-Golay smoothing technique [2]
We can write the noisy signal $y(t)$ as:

$$y(t) = x(t) + \eta(t) \tag{3.17}$$

with $x(t)$ as the original signal and $\eta(t)$ as the addictive noise; by applying the EMD, we will obtain noise corrupted IMFs, $c\eta_i(t)$.

It is possible to reduce the noise component by performing different kinds of filtering, in order to obtain "cleaner" IMFs ($\hat{c}_i(t)$); the de-noising signal $\hat{x}(t)$ can then be reconstructed as in figure 3.6, with $r_N(t)$ as the signal residue :

$$\hat{x}(t) = \sum_{i=1}^{N} \hat{c}_i(t) + r_N(t) \tag{3.18}$$

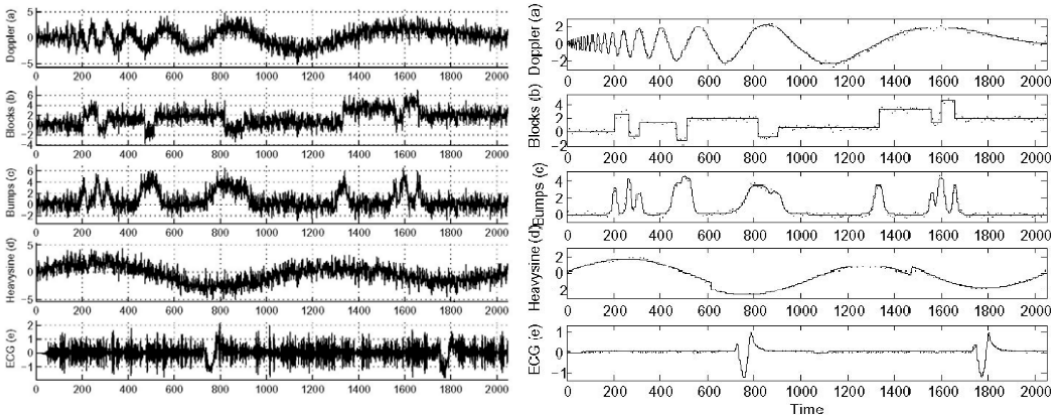

FIGURE 3.6: Example of EMD-based de-noising applied to artificial signals [6].

The Savitzky-Golay Filter

The Savitzky-Golay (SG) filter method is time-domain smoothing method that was originally designed to preserve higher moments within time-domain spectral peak data. It can be used to smooth data signals, and therefore incrementing the signal-to-noise ratio, without distorting the original shape fo the signal.
In order to achieve this result, the algorithm replaces successive sub-sets of adjacent data points with a corresponding low-degree polynomial, fitted to the data using the linear least square method.

3.3.4 Matched Filter

The previous methods served the purpose of reducing the signal noise; as we will see later, when a sufficiently clean signal is obtained, it is possible to use it as a template in order to construct a reliable detector for similar signals. To perform the actual comparison between the template and the target signal, the matched filter (MF) supervised approach can be used [20] [1] [10].
The output of a matched filter is given by equation 3.19: we can notice that, given the template h, the filter performs a linear convolution between the signal x and a time-inverted version of the template itself:

$$y[n] = \sum_{i-\infty}^{\infty} h[n-t]x[t] \tag{3.19}$$

In other words, the output y is a measure of the correlation between the template and a portion of the signal, and therefore the MF can be used to search for similarities between two different signals (if one is used as a template). In particular, y will have values that are proportional to this similarity, and thus, in order to establish if the template signal is present or not, a simple thresholding method can be applied; the output is plotted in figure 3.7.

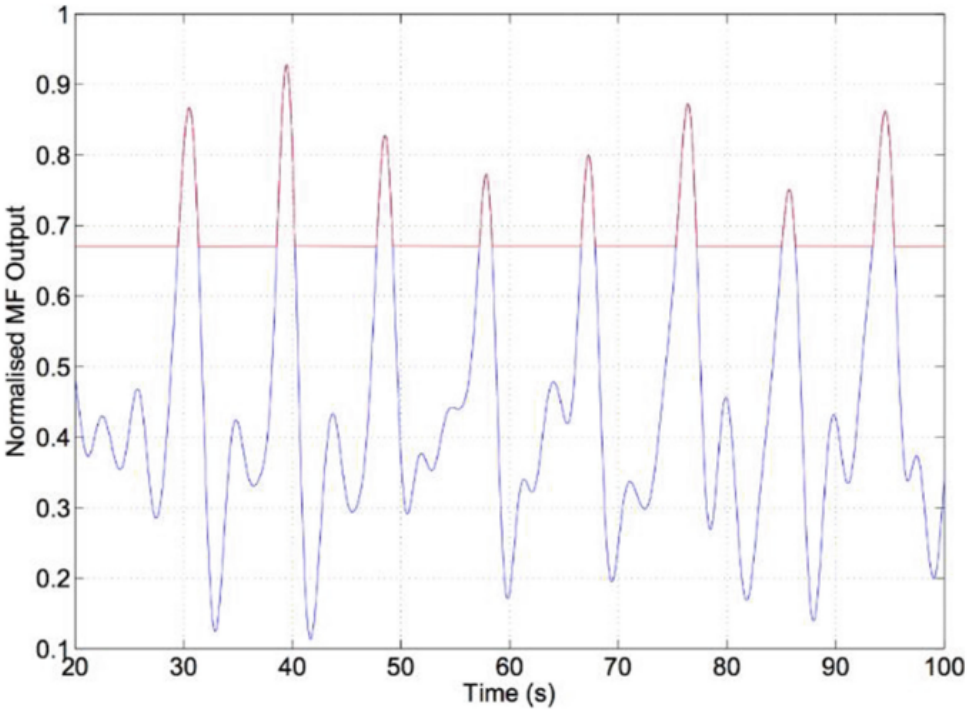

FIGURE 3.7: Example of a MF-based detector output [1].

Chapter 4

Work-flow and Results

In this chapter we will go over each part of our processing, and show the result of each phase; the goal of the whole process was to go from the raw EEG recording to the single trial evaluation of the Readiness Potential to find its presence inside a considered interval. In order to do so, we first had to make sure that our recordings contained the Readiness Potential at least by averaging over all trials: to verify this, we developed a simple algorithm to define the exact instant in which the movement started; then, we applied a simple threshold detector, improved by the TKEO operator as defined in [14] that was proven to increase the onset detection performances. After a simple band pass filter to remove the DC drift and very high frequency components, we verified - for each subject - the presence of the averaged Readiness Potential.
The RP was computed both as a simple average and by implementing the Empirical Mode Decomposition ([19] [6]) technique coupled with the Savitzky-Golay smoothing filter, which is the framework we developed for the single trial analysis.
The presence of an Event-Related Synchronization and Desynchronization were also verified in this preliminary phase: these two phenomena were computed both by using the standard method and a more recent technique that exploits the better frequency resolution offered by the wavelet transforms. In this case, no significant difference was found between the two methods, and both were sufficient to verify the ERD and ERS presence in most of our subjects.
The contemporary presence of these three signals, that were all demonstrably found in this type of experiments, was used to define a subset from all our acquisition to use as a basis for the single trial analysis: this analysis was done by the means of the above mentioned EMD-based filtering process, which was able to enhance the RP and improve the signal-to-noise ratio, coupled with a matched filter based classifier [20]. In particular, we used the enhanced RP template to find the optimal set of matched filter coefficients, so that its output would be proportional to the probability of a Readiness Potential to be present in a selected time interval.
The detailed process for each step is reported in the sections below, together with the obtained results.

4.1 EMG Onset Detection

Given the raw EEG signal, the first step of our process was to determine the exact instant in which the finger movement was initiated. In order to do so, we applied techniques mentioned in chapter 3.1 to the raw EMG recording.
First, we used algorithm 1 to remove slow trends and high frequency noise

Algorithm 1 EMG filtering

1: Resample @128Hz;
2: Remove mean and slow trends;
3: Notch filter @50Hz to remove power line interference;
4: Low pass filter @40Hz.

from the EMG; secondly, we implemented a simple threshold detector after applying the TKEO operator and computing its derivative. The threshold in algorithm 2 was determined as follows:

$$Threshold = u_0 + j \cdot \delta_0 \tag{4.1}$$

where u_0 and δ_0 were respectively the mean and standard deviation of the signal, computed in a baseline period, which was determined as the first half second of our window; j was set at 1.5.
After the detection, each onset time-point was stored as a property of the EEG structure and will be later used to epoch the continuous recording. An example of onset detection is reported in figure 4.1.

Algorithm 2 Onset Detection

1: Apply the TKEO operator;
2: Find the EMG peaks;
3: Extract $[-2s \div 0s]$ windows referring to each peak;
4: Compute the first derivative of each window;
5: Find the first sample above *threshold*, mark it as onset.

4.2 EEG preprocessing

After marking the onset time of each epoch, we proceeded to filter the EEG recordings; for each channel, we implemented a high pass filter with cut-off frequency of 0.01 Hz, in order to eliminate the slow DC drifts, and a low-pass filter at 30 Hz. The filters' impulse responses are reported in figures 4.2 and 4.3.
In accord with most literature, both filters were chosen as linear phase FIR filters. By doing so, we could easily compensate the filter-introduced delay, by simply computing the linear phase delay and shifting the signal accordingly; this step was necessary, as we are interested in a very specifically time-locked event, and therefore we had to be careful not to introduce any phase shift during the filtering process.

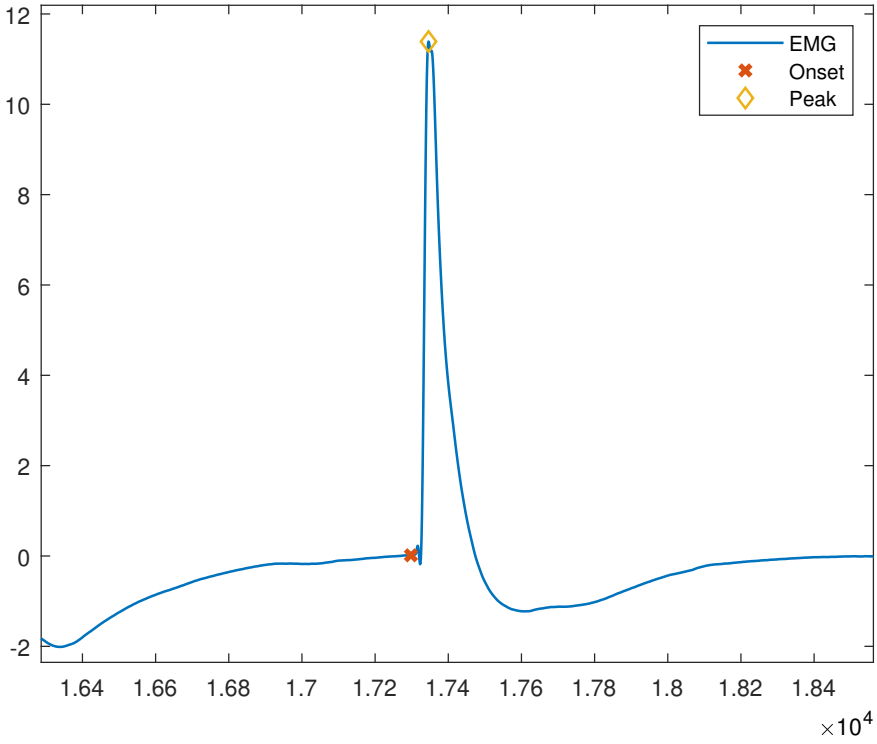

FIGURE 4.1: One epoch of the EMG is plotted, together with the peak and onset point found by our algorithm.

Algorithm 3 EEG Filtering

1: Resample @128Hz;
2: Apply high-pass FIR filter, with cut-off frequency of 0.01 Hz;
3: Linear delay compensation;
4: Apply low-pass FIR, with cut-off frequency of 30 Hz;
5: Linear delay compensation.

4.3 Event-Related Synchronization and Desynchronization

After filtering the EEG, we studied its event-related synchronization and desynchronization; to do so, we applied and confronted two methods: the classic band power method as described by Pfurtscheller in his original papers [25] [24] [21] [23], and a more recent method based on the Morlet Wavelet Transform [3]. Algorithm 4 and algorithm 5 synthesize these procedures.
From literature, we expected to find a de-synchronization in the alpha band (between 8 Hz and 12 Hz), with corresponding decrease in power, and a synchronization in the beta band (between 26 Hz and 30 Hz), with a corresponding increase in power. The ERD is expected to start about two seconds before the onset, while the ERS should start immediately after the movement is initiated.

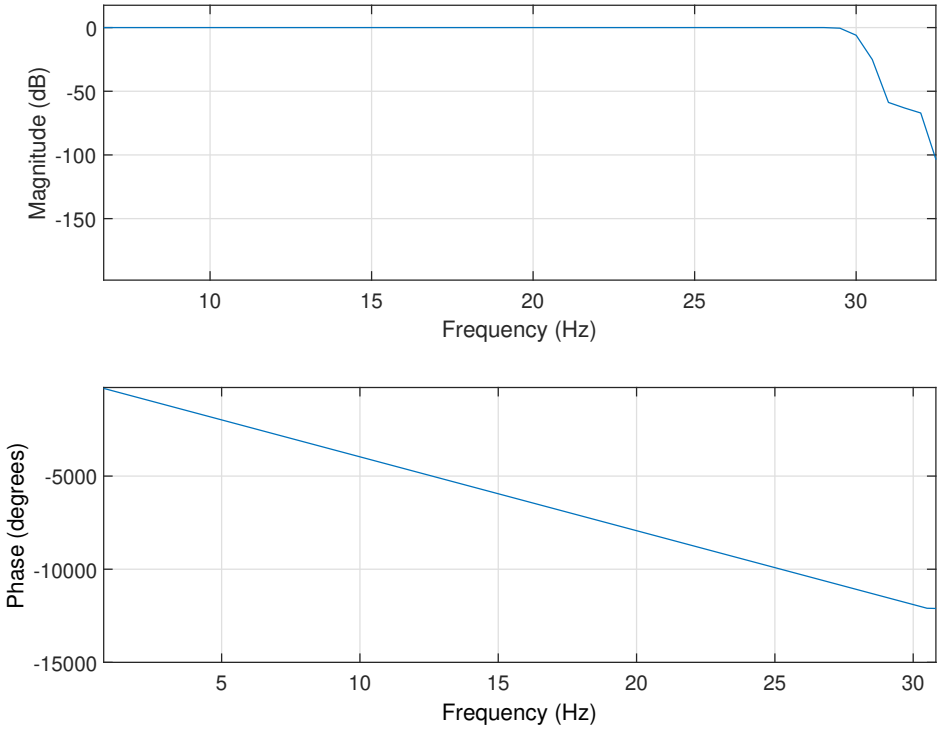

FIGURE 4.2: Low-Pass FIR filter: impulse response and phase.
This filter was used to process the EEG.

As we can see from the grand average plots in figure 4.4, the results are overall coherent with what was expected, with a decrease in alpha power starting about 2 seconds before the onset and a subsequent increase in the beta band. Reported below is a list of plots showing the ERD and ERS for some of our subjects, plus the grand average plot across all subjects.

Algorithm 4 ERD/ERS Band Power Method

1: **for** each epoch **do**:
2: Band pass between $lowfrequency$ and $highfrequency$;
3: Squaring of the amplitude samples to obtain power samples;
4: Averaging of power samples across all trials;
5: Averaging over time samples to smooth the data and reduce the variability.
6: **end for**
7: Compute the mean power of the reference interval R $(-3.5s \div -2.0s)$;
8: $ERD/S\% = 100\frac{(A-R)}{R}$.

4.3.1 ERD and ERS Plots

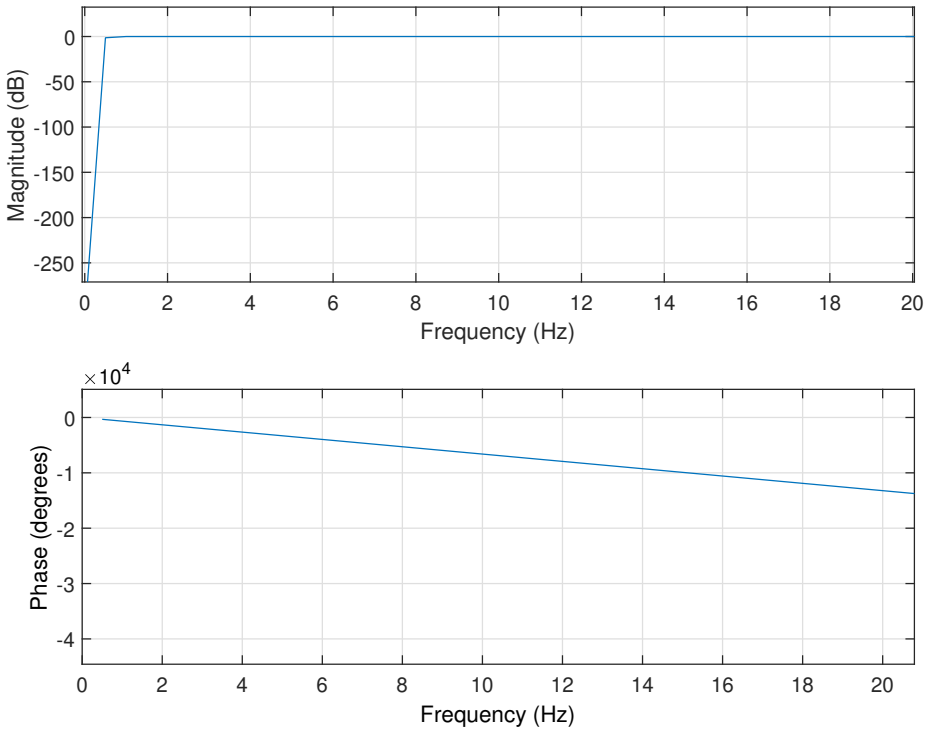

FIGURE 4.3: High-Pass FIR filter: impulse response and phase.
This filter was used to process the EEG.

Algorithm 5 ERD/ERS Morlet Wavelet Method

1: **for** each epoch **do**:
2: Perform the Morlet CWT decomposition;
3: Find all frequencies lying in the selected frequency band;
4: Square the absolute value of the result to obtain instantaneous power samples;
5: **end for**
6: Compute the mean power in the reference interval R $(-3.5s \div -2.0s)$;
7: $ERD/S\% = 100\frac{(A-R)}{R}$.

Grand Averages

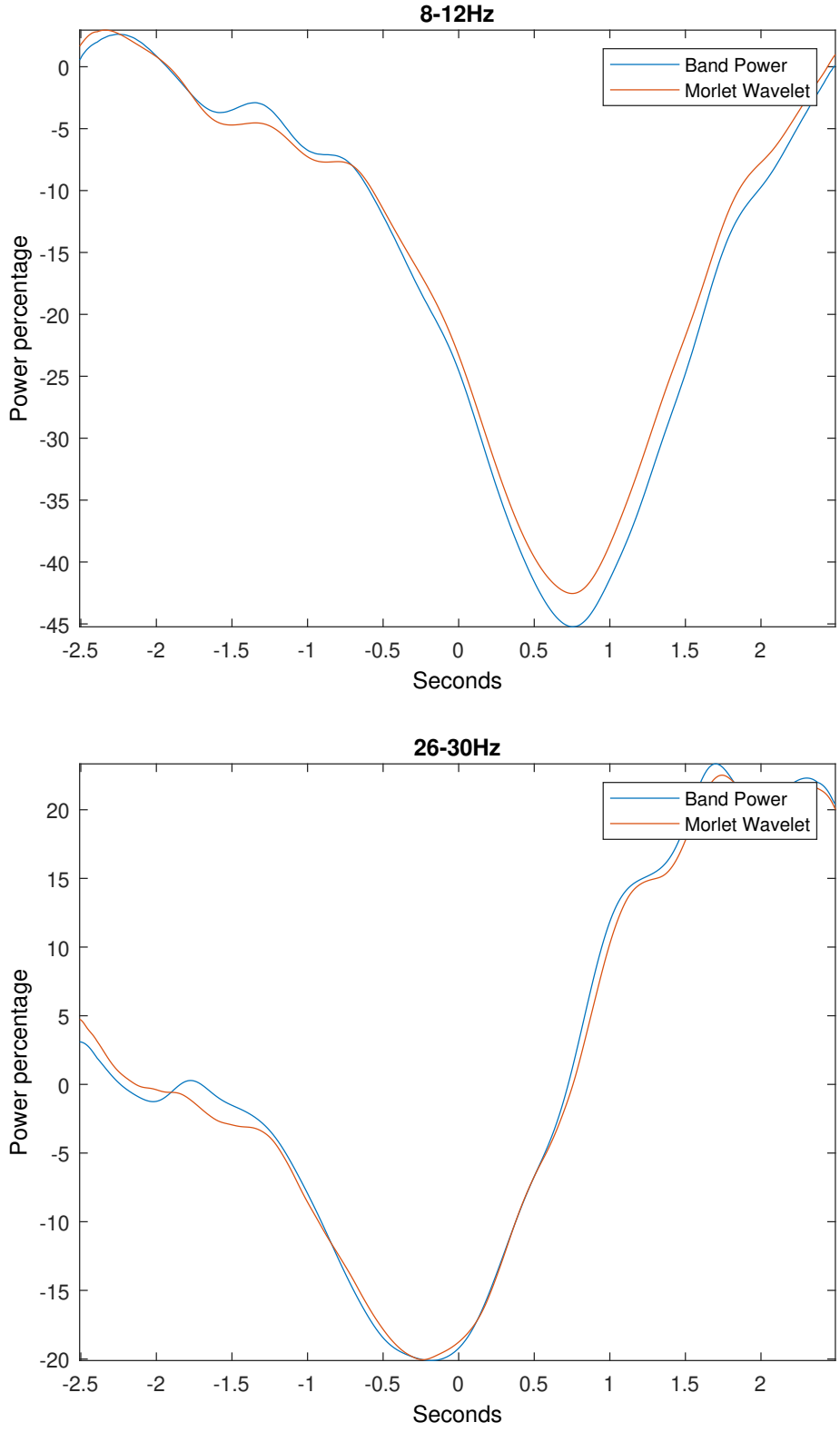

FIGURE 4.4: The ERD and ERS grand averages across all experiments.

Subject 1

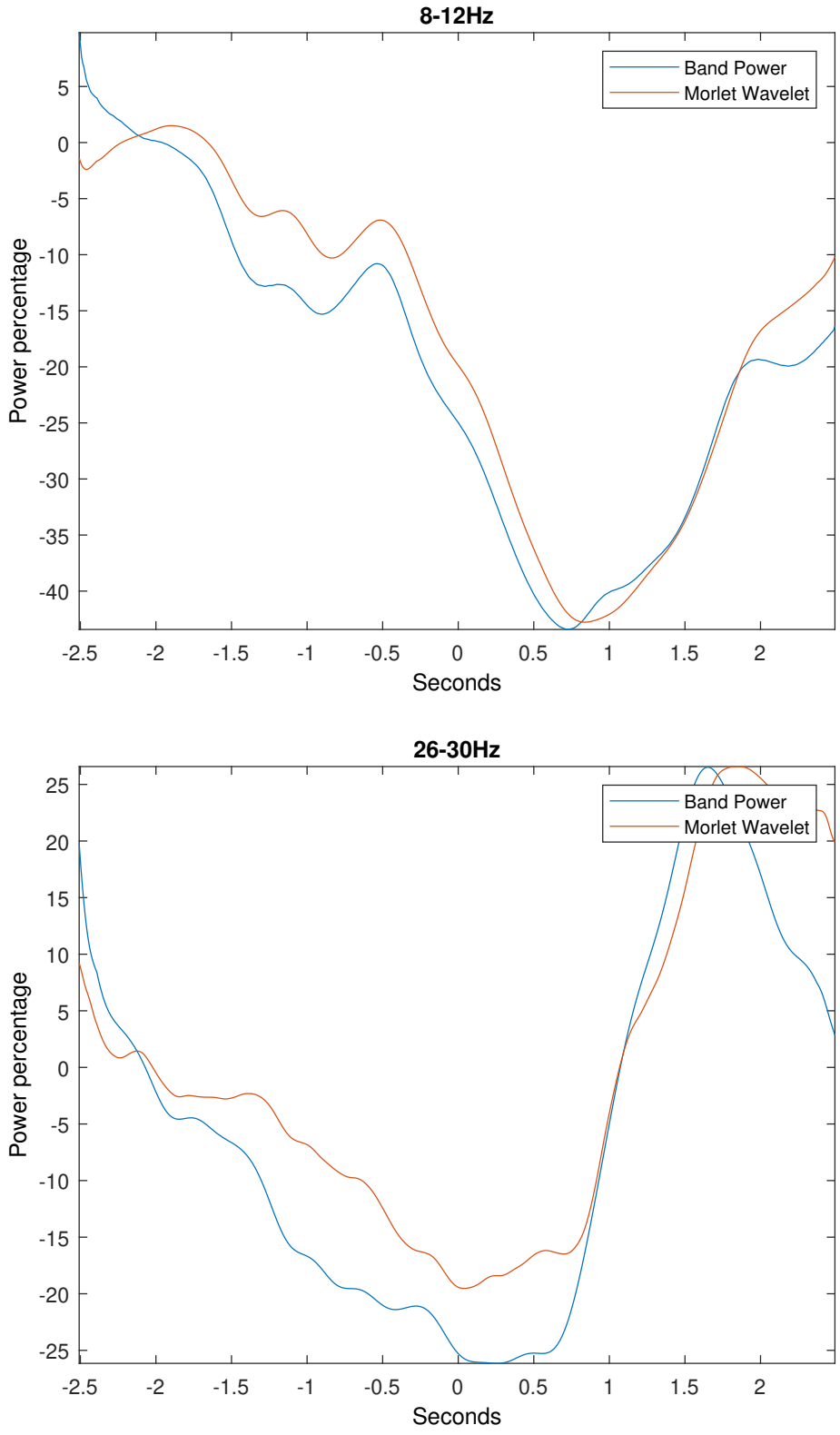

FIGURE 4.5: ERD and ERS plots on subject 1.

Subject 2

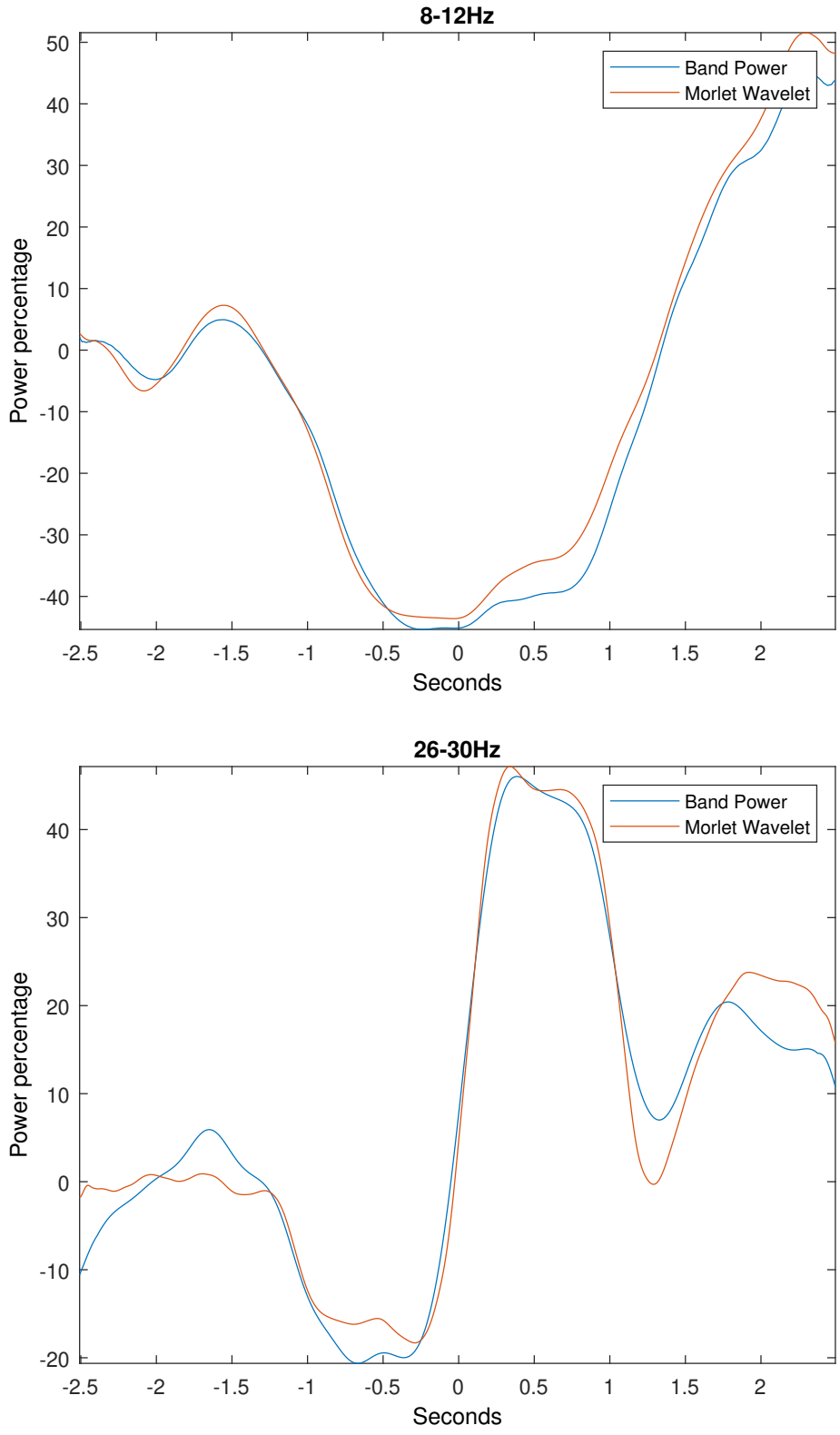

FIGURE 4.6: ERD and ERS plots on subject 2.

Subject 3

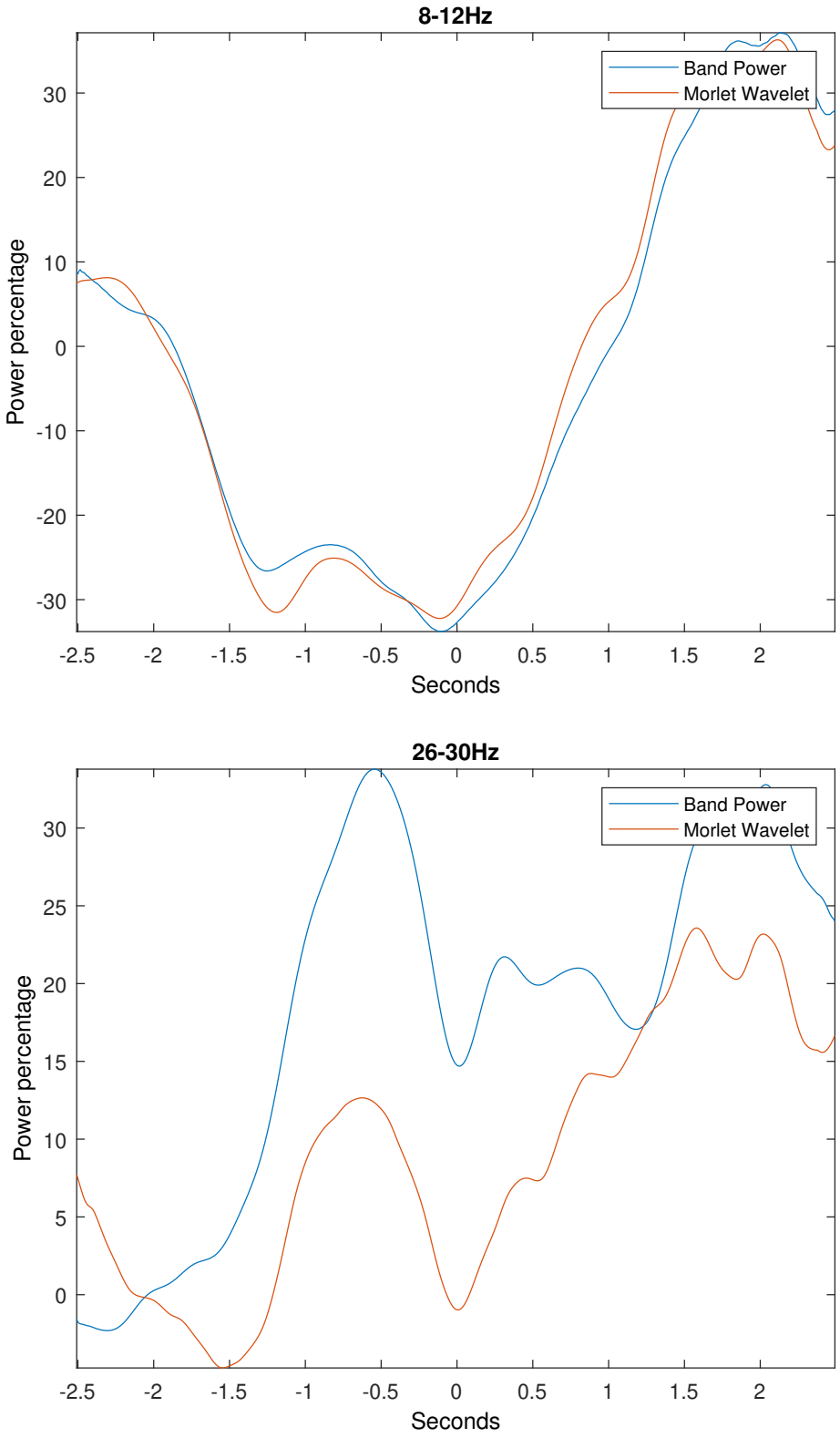

FIGURE 4.7: ERD and ERS plots on subject 3.

Subject 18

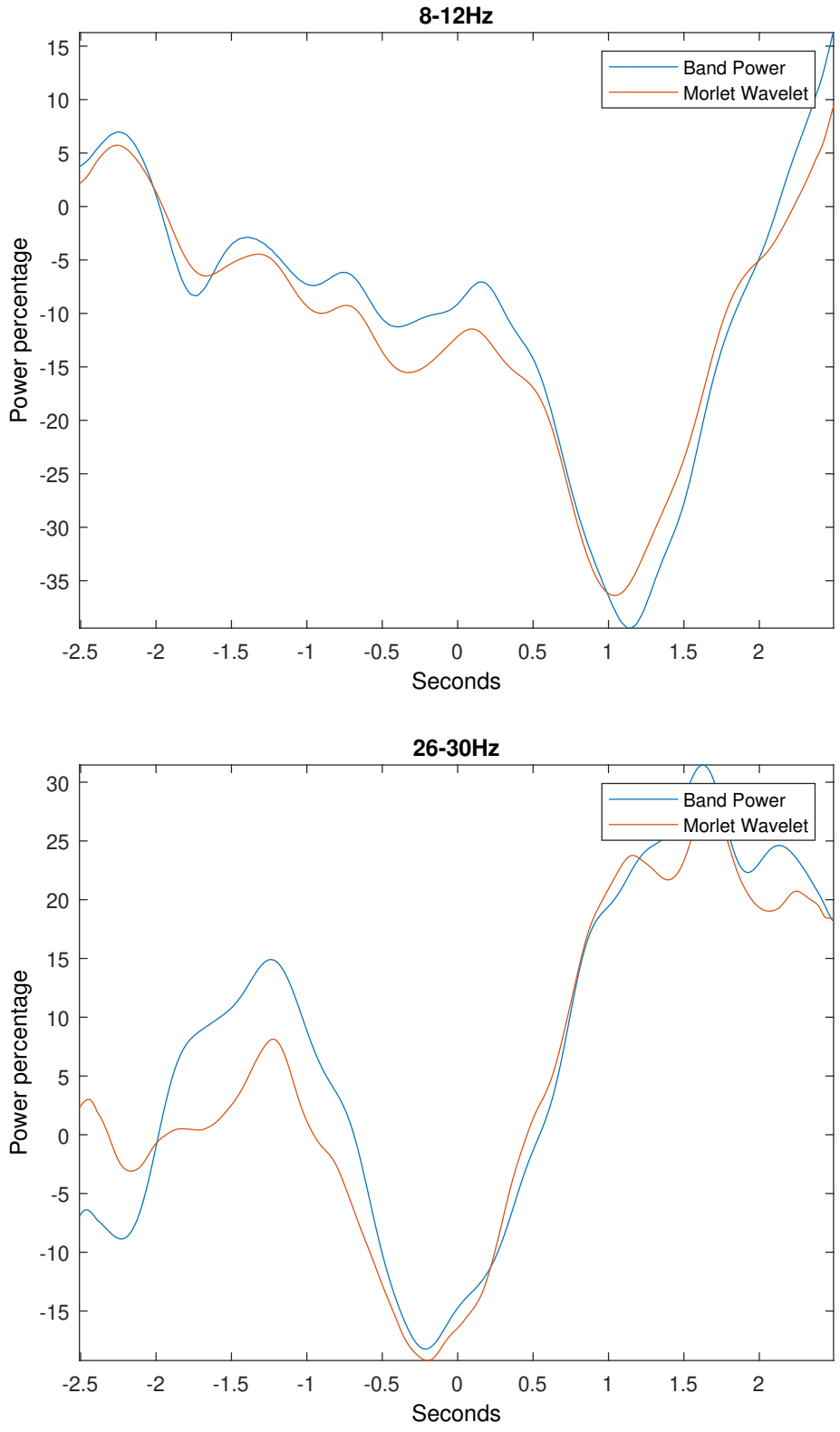

FIGURE 4.8: ERD and ERS plots on subject 18.

Subject 20

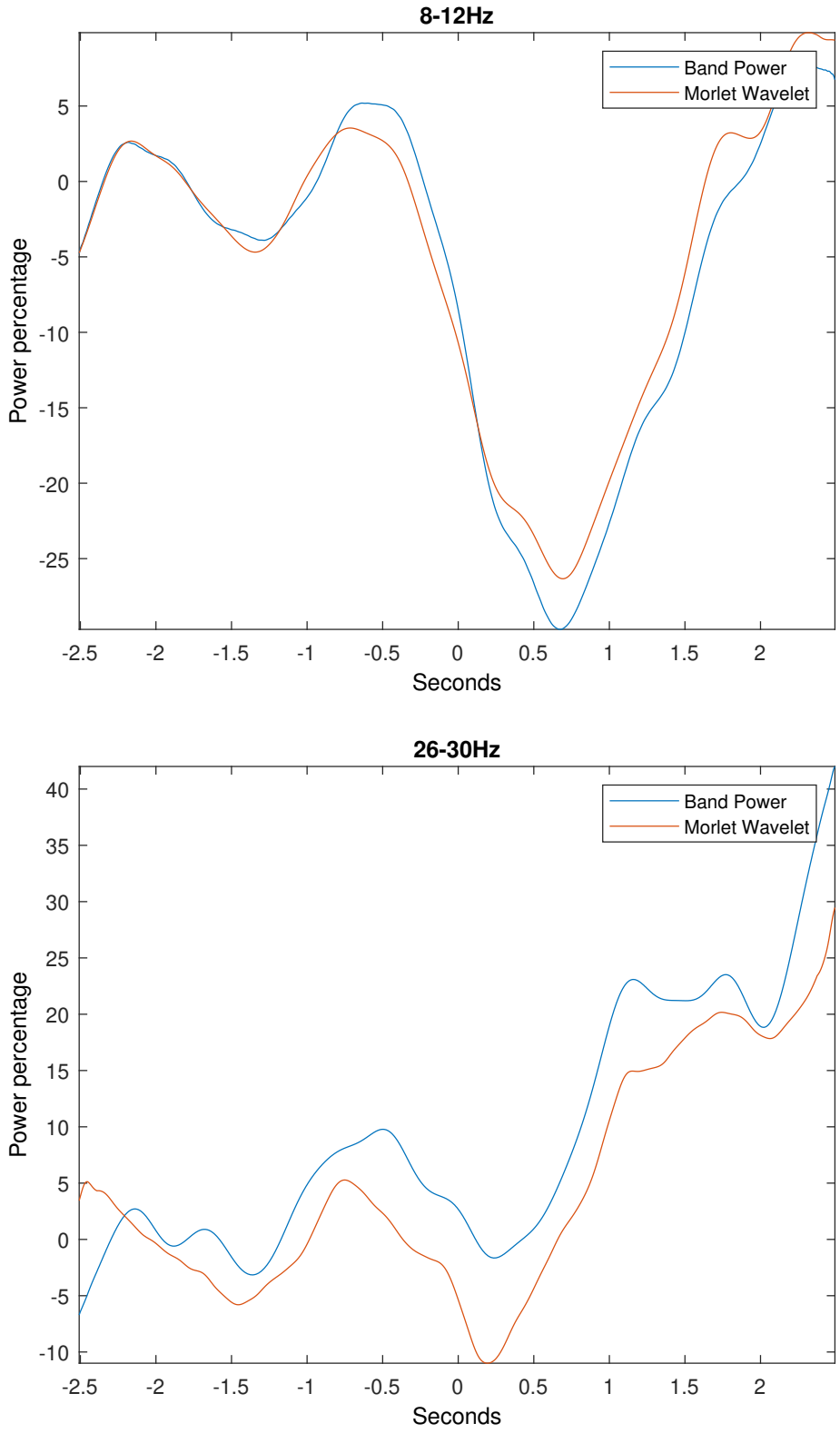

FIGURE 4.9: ERD and ERS plots on subject 20.

Subject 27

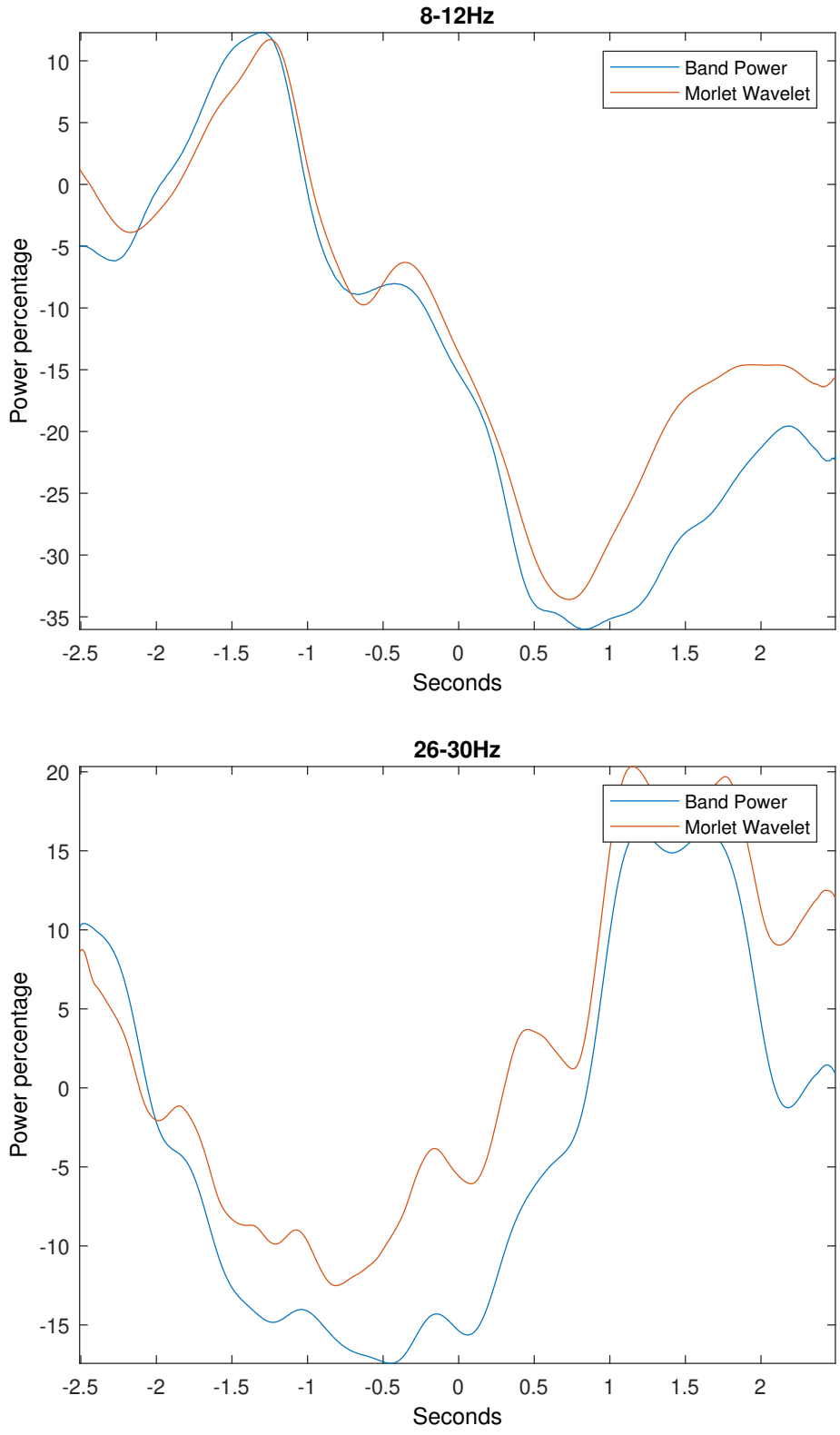

FIGURE 4.10: ERD and ERS plots on subject 27.

4.4 Averaged Readiness Potential

Together with the ERD and ERS study, we also computed the averaged signal on the acquired dataset; computing the average had two main purposes: first, we needed to assess the validity of our acquirements, and second we could begin to evaluate our EMD method by comparing the simple average with the EMD average.
Algorithm 6 summarizes the processing method: the Empirical Mode Decomposition was applied on a surrogate channel created by running a large laplacian filter on the central electrode (for our purposes, *Fc3*); the spatial filter was demonstrated to reduce the spatial noise [17].
The most important step of our analysis was the removal of the first three EMD components; this method was proven to enhance the SNR, without removing important information regarding the RP signal [11] [4]. To further reduce the noise, each component retrieved by the EMD technique was smoothed using a Savitzky-Golay filter before reconstructing the signal, as suggested by [6].

Algorithm 6 Spatial Filter + EMD + Savitzky-Golay Framework

1: Select the central channel (Fc3);
2: Compute the surrogate channel by applying the large laplacian spatial filter 3.16;
3: **for** surrogate epoch **do**:
4: Compute the EMD modes (algorithm 3.3.2);
5: Apply the Savitzky-Golay filter on every mode to further reduce noise;
6: Sum all modes minus the selected first few to obtain a filtered epoch;
7: **end for**
8: Average over all epochs.

4.4.1 Averaged RP Results and single-trial subset selection

These plots offer a first example of the effectiveness of our framework: from visual inspection we could verify that, in most cases, the EMD - coupled with the spatial filter - was able to enhance the RP. To proceed with single trial evaluation, we selected a subset from both our datasets (old and new protocol): the RP was clearly visible in 13 out of 22 acquisition from the new database, and in 15 out of 19 from the old database.
As we can see from the plots, removing four EMD components renders the signal quite unclear, while removing three appears to be the best case, concordant with the results found in [11] and [4].
All Readiness Potentials are conventionally plotted upside-down.

Grand averages

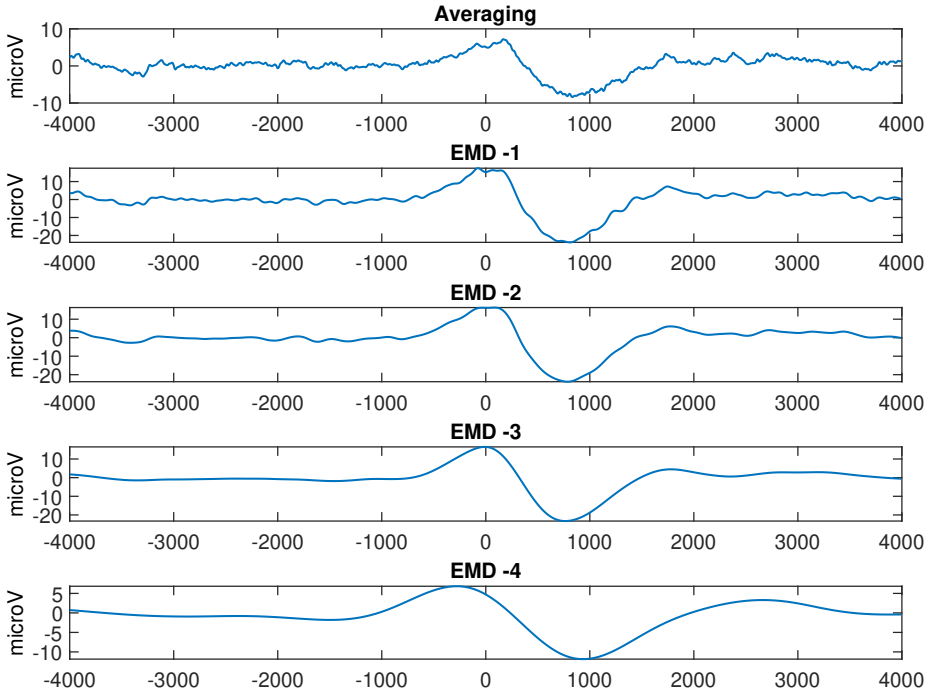

FIGURE 4.11: Grand Average RP plots; we can see from both figures that removing three components has the best performances.

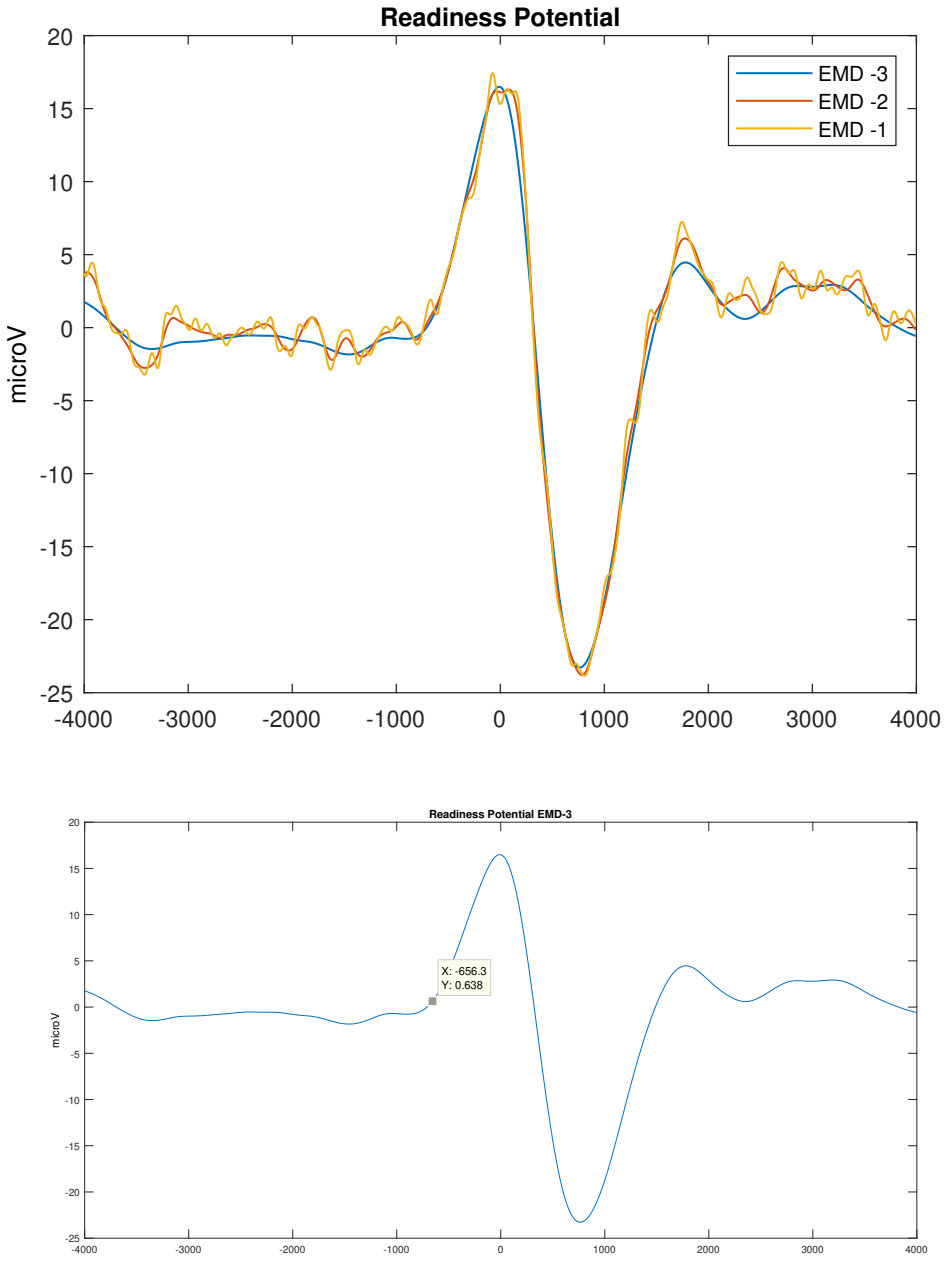

FIGURE 4.12: Grand Average plot of the Readiness Potential; the onset time is highlighted.

Subject 4

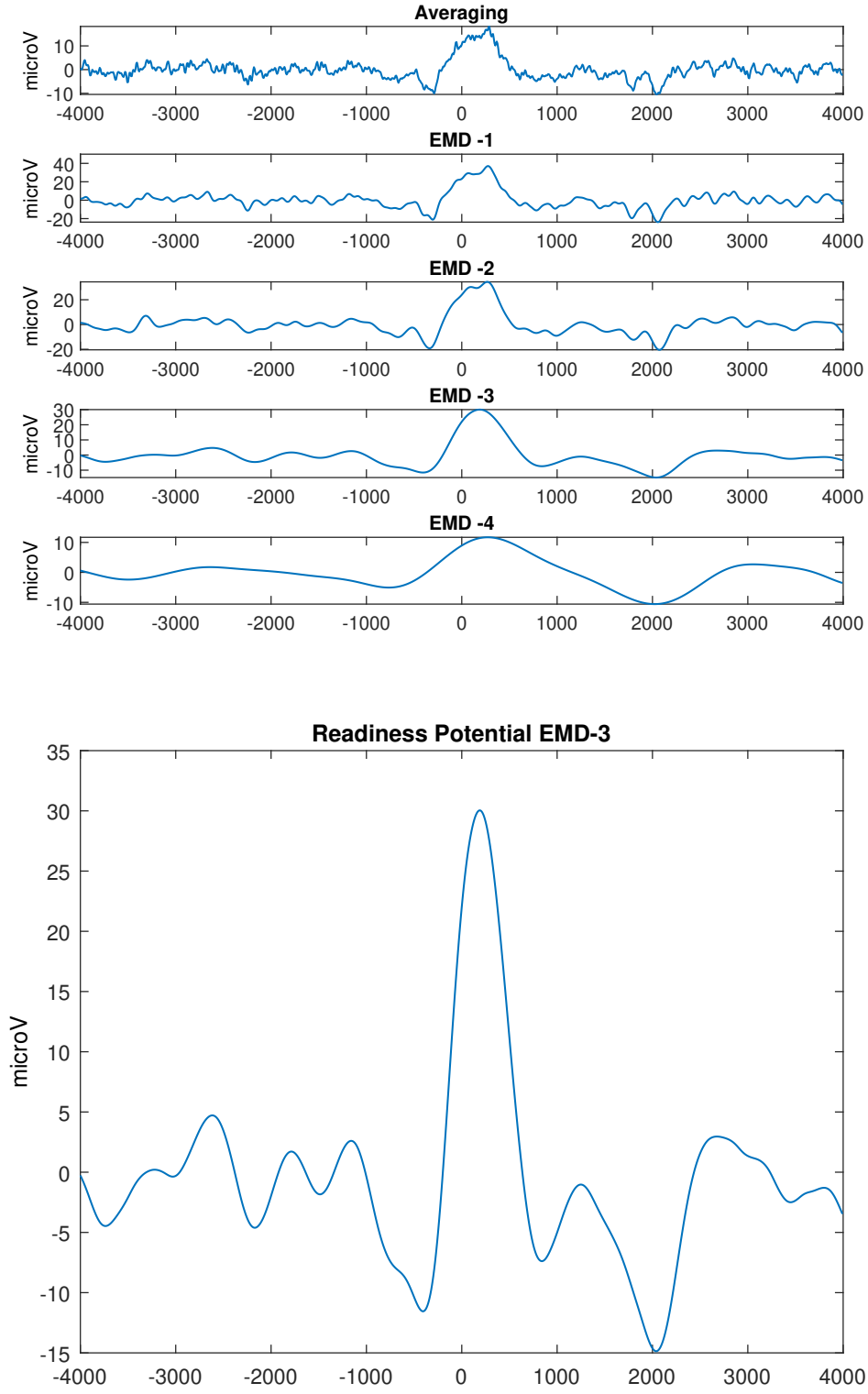

FIGURE 4.13: RP plot on subject 4.

Subject 7

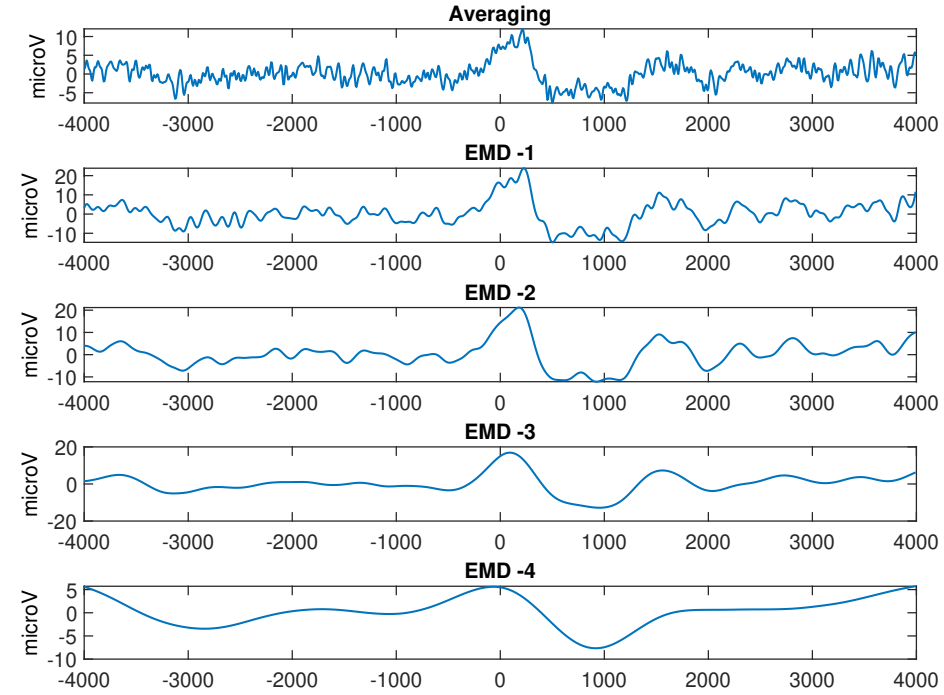

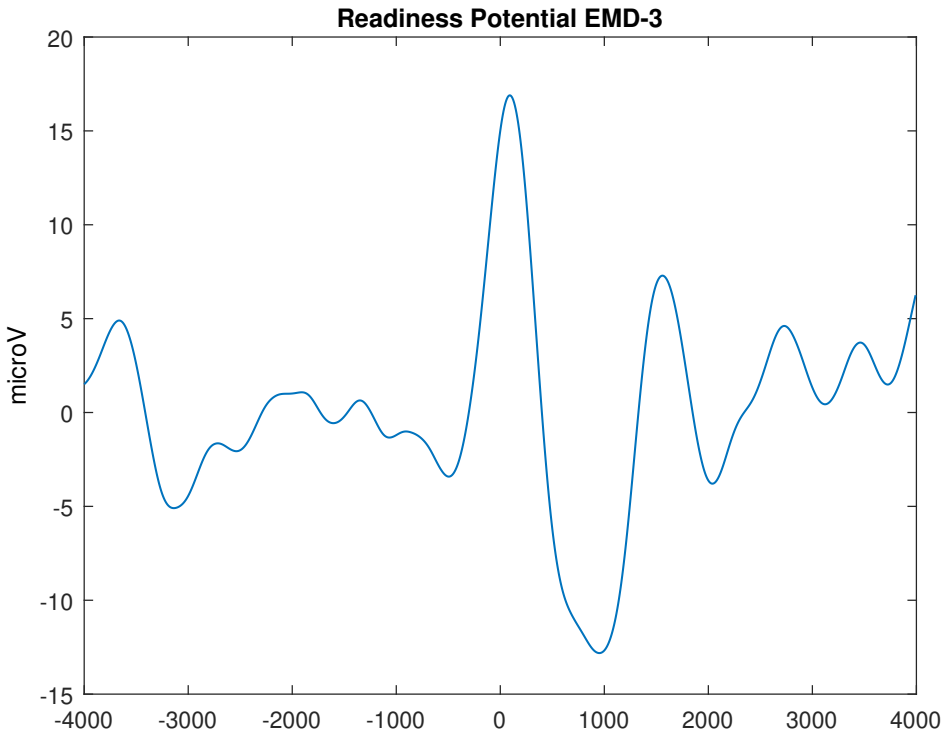

FIGURE 4.14: RP plot on subject 7.

Subject 13

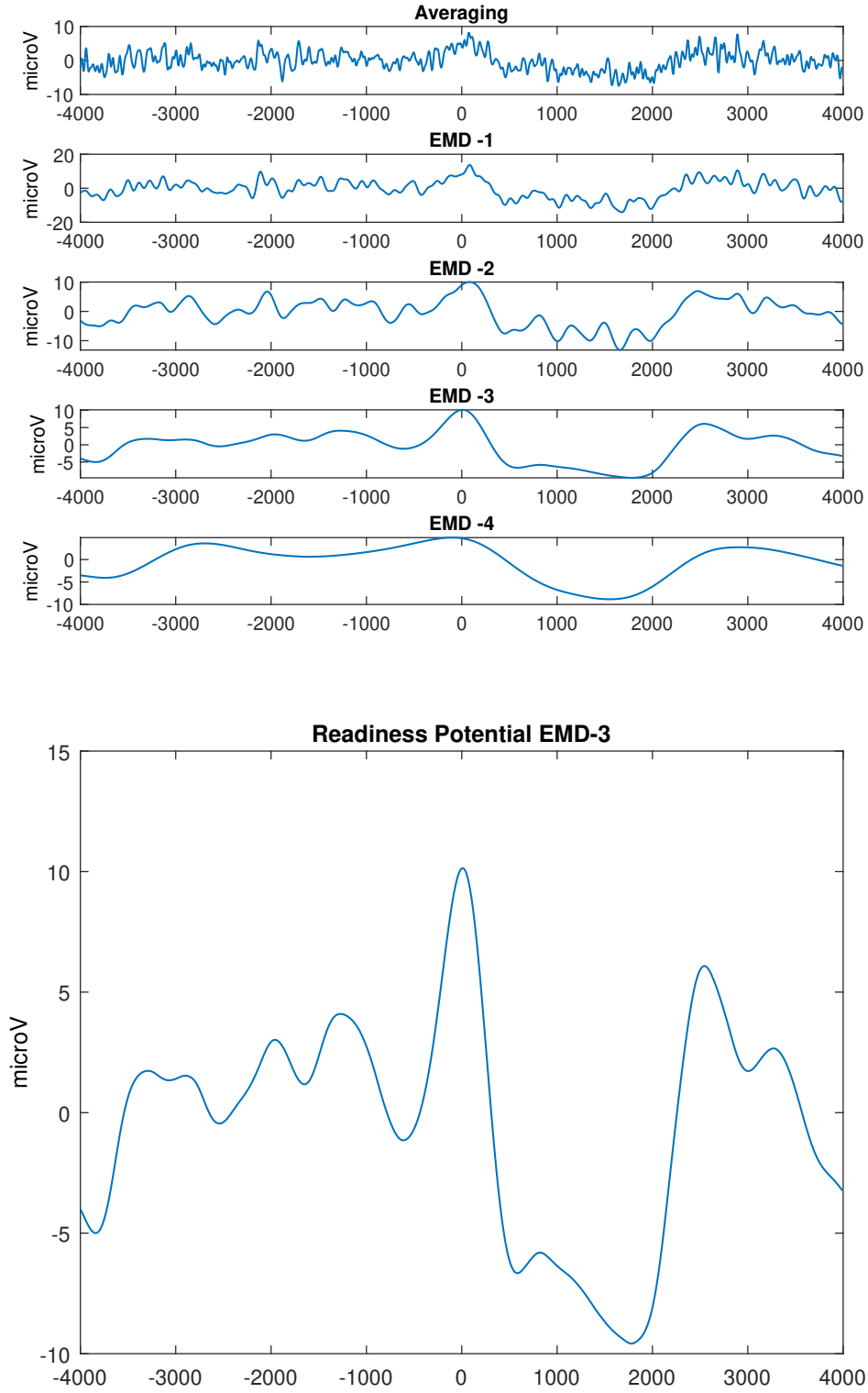

FIGURE 4.15: RP plot on subject 13.

Subject 17

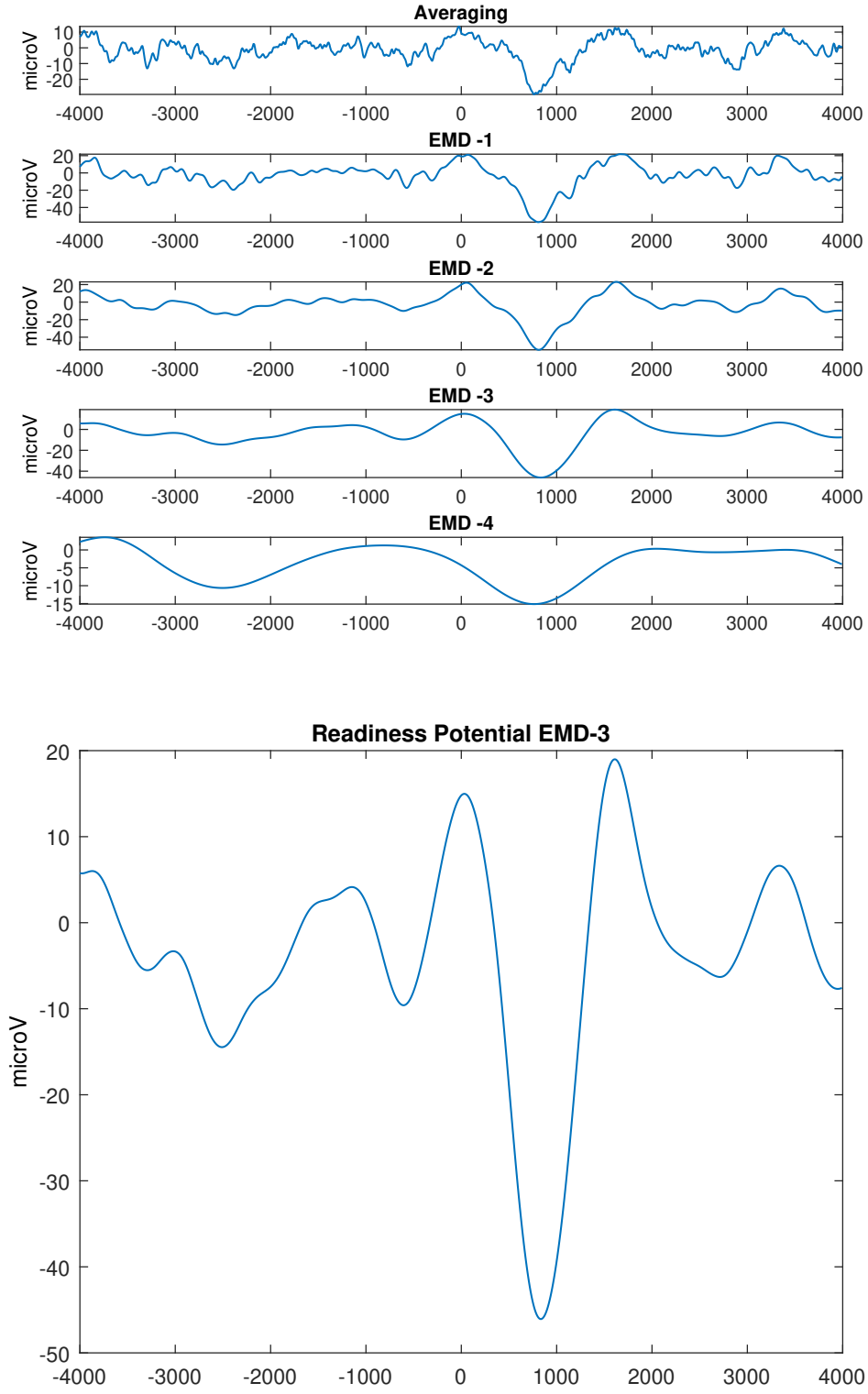

FIGURE 4.16: RP plot on subject 17.

Subject 23

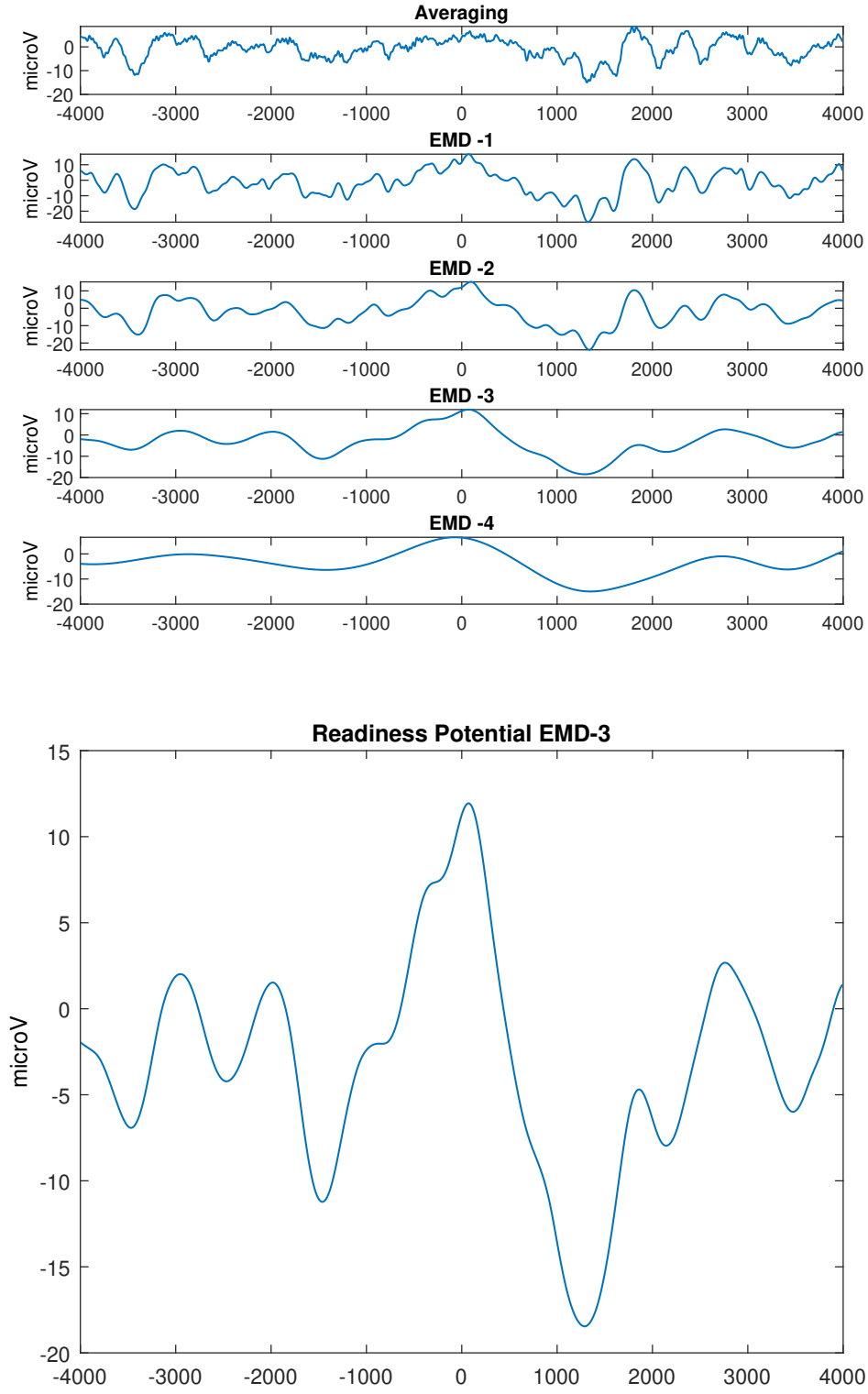

FIGURE 4.17: RP plot on subject 23.

Subject 25

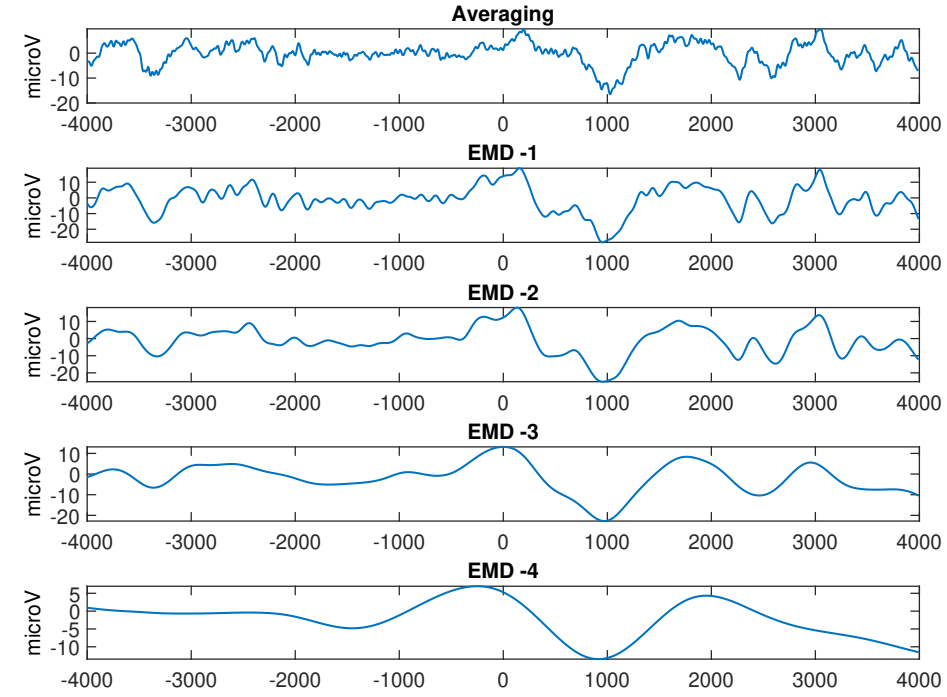

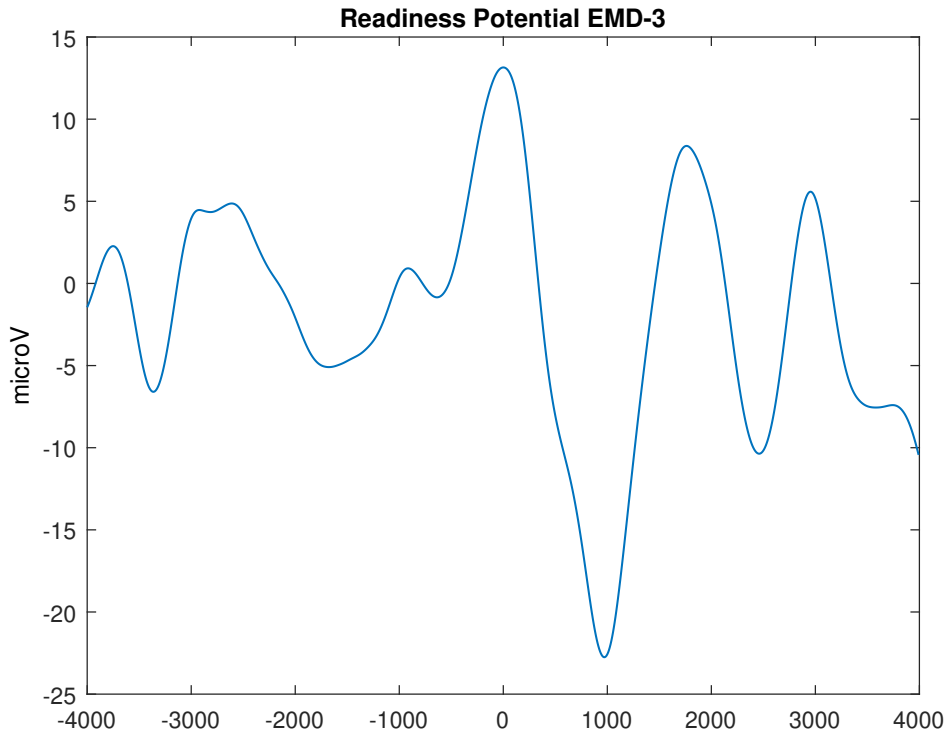

FIGURE 4.18: RP plot on subject 25.

4.5 Matched Filter and Single Trial

4.5.1 Select the Template

In order to create the matched filter detector, we first need to extract its coefficients from our training data. These coefficients are nothing but the signal we want to detect, and the matched filter output is a measure of the correlation between our template and the filtered window, as explained in section 3.3.4. We created the template - the filter coefficients - as an average of a number of epochs randomly selected from our training set.
The algorithm below was developed to find the minimum number of epochs to average in order to compute a reliable template. We used the euclidean distance as a measure of fitness to quantify the diversity between templates created by an increasingly high number of epochs: imposing a maximum distance of 0.01%, we found that no more than 45 epochs were needed. Thus, we decided to use 70 epochs in order to create the template, and the remaining epochs could be used as a validation set.
By averaging 70 randomly chosen epochs from our database, we obtain the

Algorithm 7 Template Selection

```
for epoch do:
    Compute the EMD filtered signal as per 6;
    for i = 5 : 5 : NumEpochs do
        for j = 1 : NumValid do
            Randomly select i epochs;
            Average the selected epochs to create a possible template;
            Save the template;
        end for
        Compute the euclidean distance between all NumValid templates;
        Select the first i with a fitness value lesser than 0.05%.
    end for
end for
Save i.
```

template reported in figure 4.19: as we can see, despite using only a limited number of epochs, the template appears to be much similar to the grand average 4.11. Thus, we selected the last 2 seconds before the EMG onset as coefficients of the matched filter.

4.5.2 Train the Linear Classifier

Now that we obtained the coefficients of the matched filter, we can run it through our database and train a basic linear classifier to discriminate between windows containing the RP and windows without the RP.
In order to do that, we ran the matched filter on the remaining database (the epochs used to create the template were eliminated); then, we took 30% of

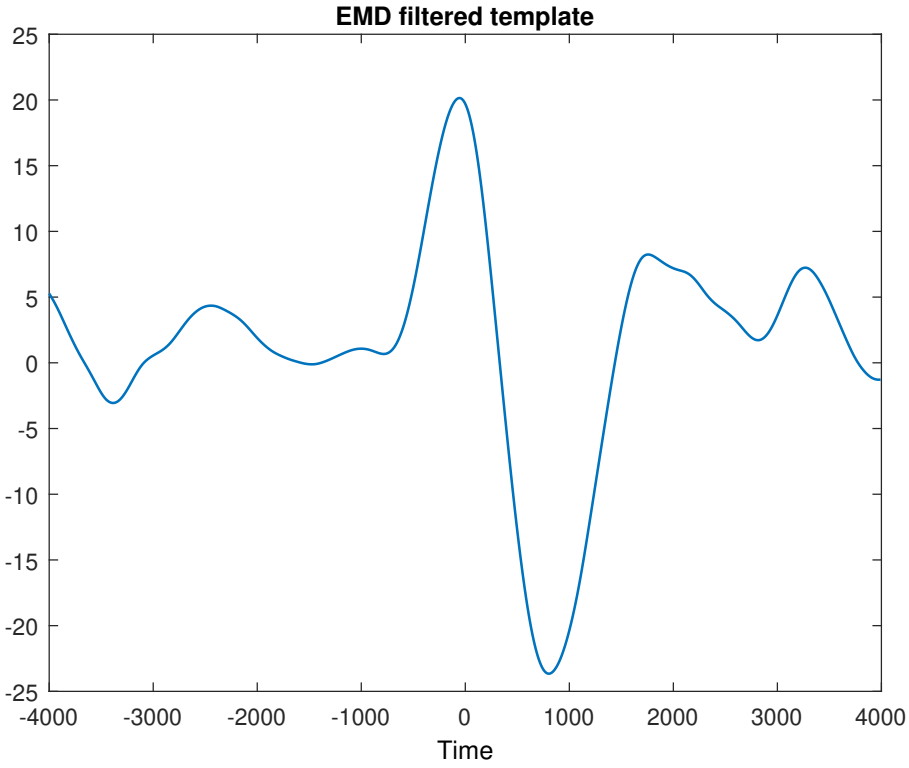

FIGURE 4.19: The average over 70 randomly chosen epochs, filtered with the EMD process. The matched filter coefficients were chosen as the section from -2s to 0s.

it as training set and divided each epoch in 2 second windows. We considered as positives the windows before the EMG onset, and as negatives the remaining areas. Then, for each window, we saved 5 time-samples, 0.5 seconds apart, and trained a simple linear classifier using the time-samples as features.

The confusion matrix in figure 4.21 shows the ability of our classifier to discriminate between positives and negatives, as defined above; the results are obtained after running the linear classifier on the other 70% of our initial data. As we can see, the overall accuracy is close to 70%.

Below we reported the detected RPs on some single trial epochs: as we can see, the number of false positives is still quite high, but the majority of them is located in the second part of the epoch, after the movement. These false positives are less important than FPs found in the first half, as they could pick up cerebral activity related to the movement itself, that shouldn't be present in paralysed patients.

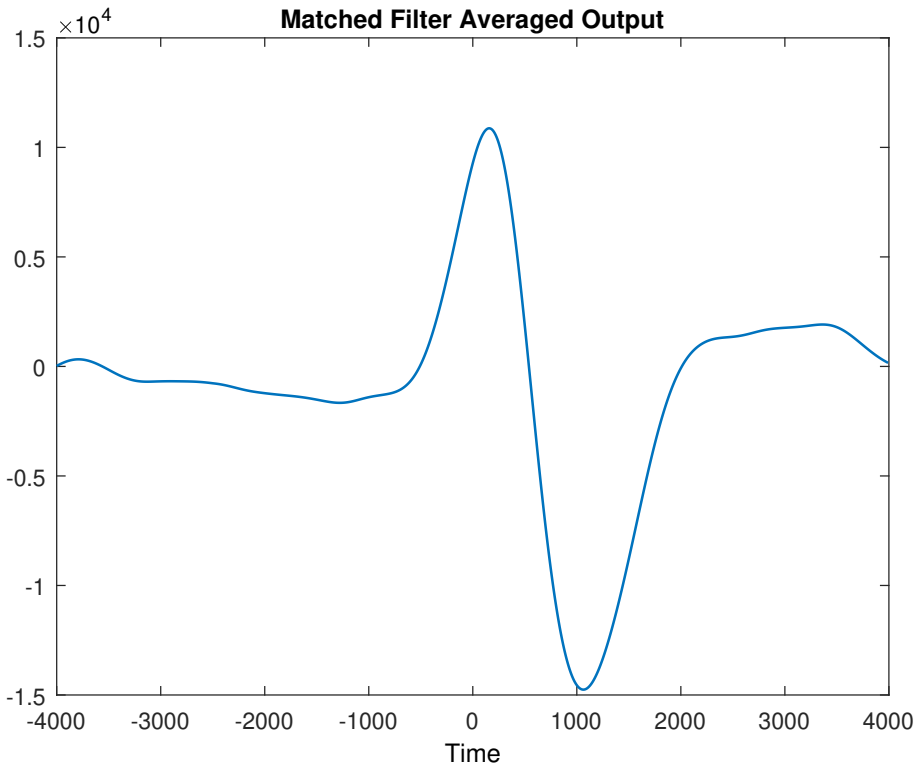

FIGURE 4.20: Plot of the average matched filter output on 150 epochs: the averaged result confirms what we expected, with a maximum of intensity corresponding to the EMG onset.

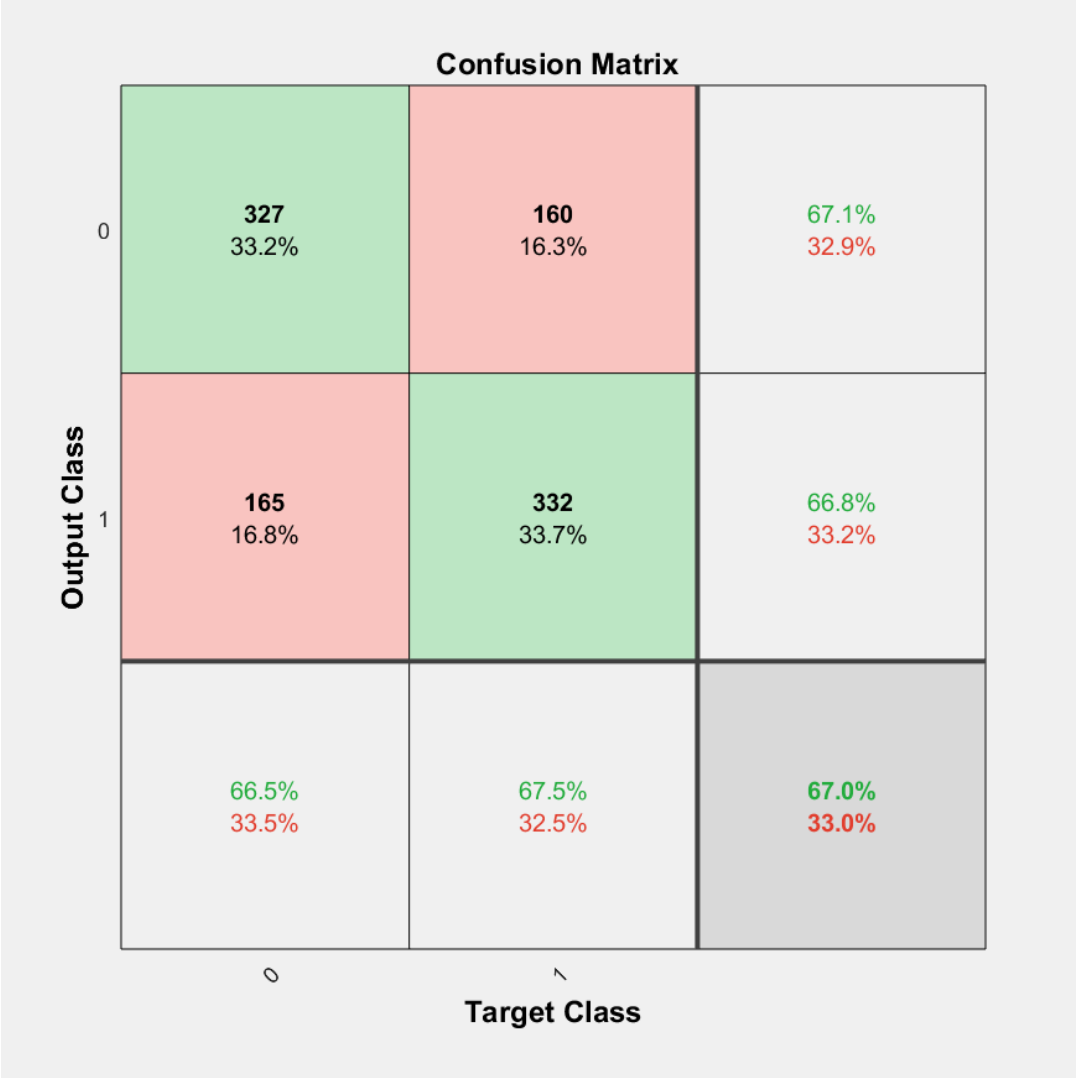

FIGURE 4.21: The confusion matrix of the linear classifier. The output labelled as 1 are the RP containing windows, and vice versa.

Random Epoch 1

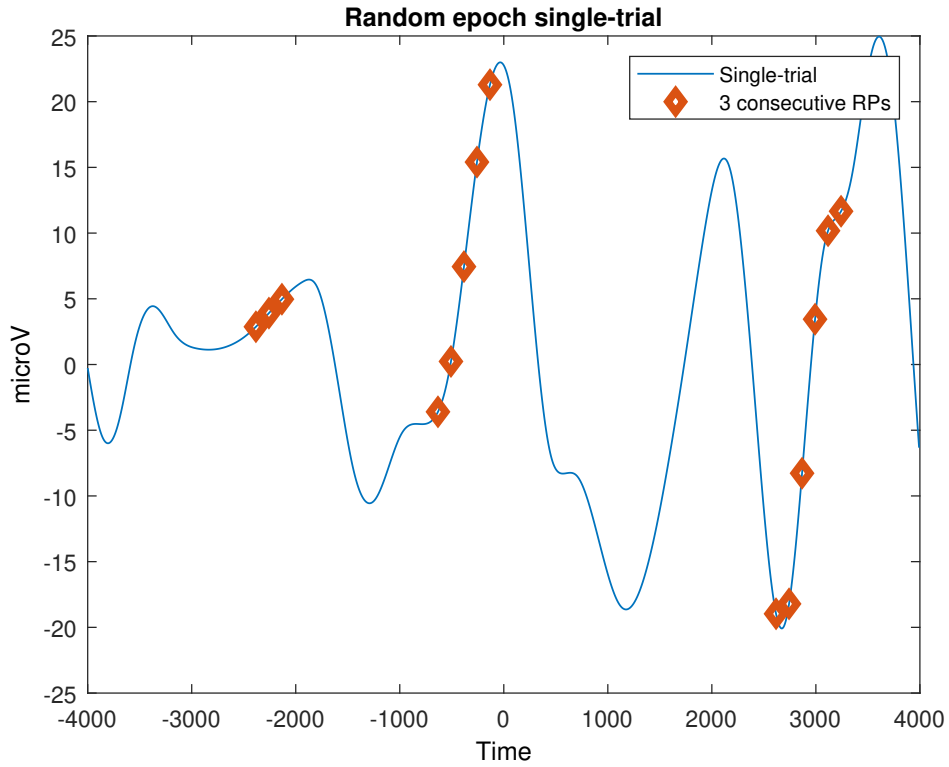

FIGURE 4.22: Single-trial RP detection.

Random Epoch 2

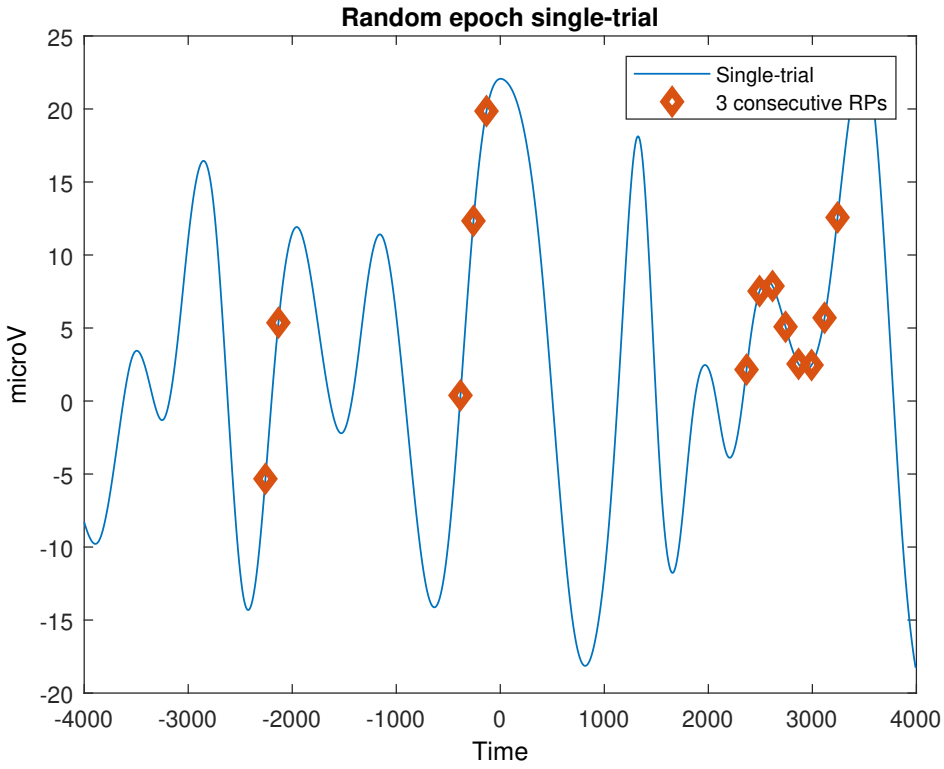

FIGURE 4.23: Single-trial RP detection.

Random Epoch 3

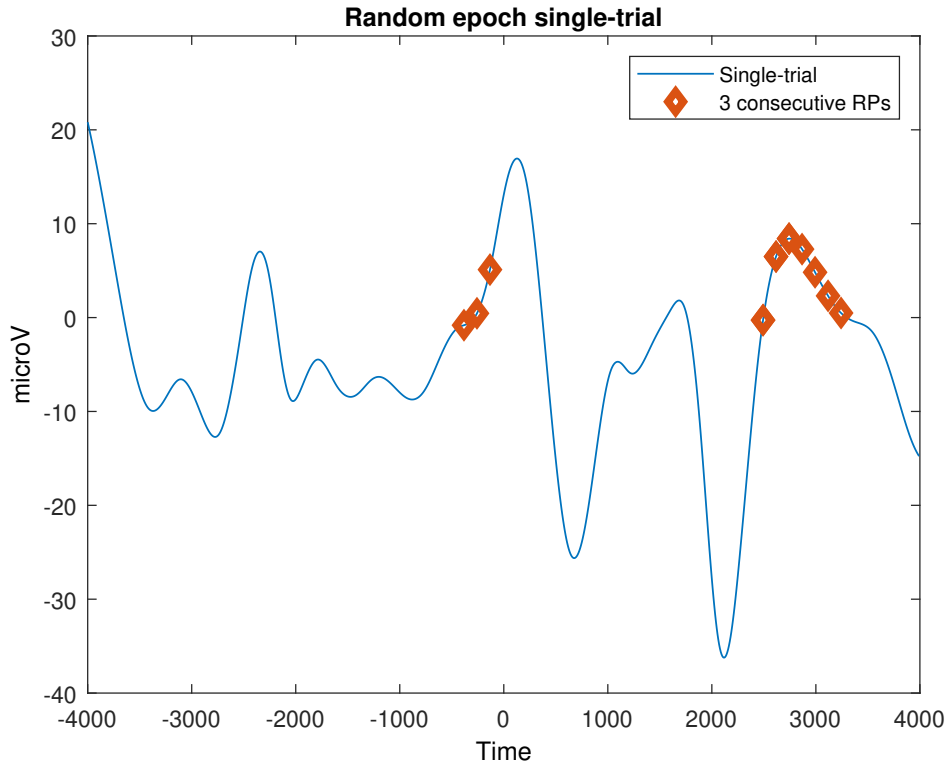

FIGURE 4.24: Single-trial RP detection.

Chapter 5

Conclusions

The Empirical Mode Decomposition technique has proven to be an effective method to remove most of the noise from the EEG signal, in order to enhance the presence of Readiness Potentials; we were able to find the RP deflection in 60% of the new acquisition database, and 78% of the old dataset. In all cases, even when the RPs were visible by simple averaging, the EMD allowed for a better signal quality.
The Event-Related Synchronization and De-synchronization was also present in most of the trials that clearly contained the RPs, with no significant difference between the two proposed methods (band power technique and Morlet Wavelet technique); the simpler band power method had proven to be sufficiently accurate to perform this analysis.
As far as the single-trial analysis, our proposed method based on a matched filter classifier was able to discriminate correctly the 68% of 2 seconds windows in our validation set, which in an encouraging result. Overall, the task of accurately detect the RP presence without the means of an averaged technique remains a challenging problem, and the following considerations should be made as a suggestion to improve the performances compared to our work.
First, the need for a sophisticated preprocessing paradigm emerged: our basic filtering scheme had adequate performances when it came to analyse averaged quantities and signals, but, in order to enhance the single-trial efficiency of any method, the preprocessing phase should include state-of-the-art artefact removal procedures.
Secondly, we should highlight an intrinsic limit of a matched filter technique based on a template RP: the ultimate goal of our study is to detect the RP in Vegetative State (VS) and Locked-In Syndrome (LIS) patients: the RPs present in these conditions are not guaranteed to be identical to those found in healthy patients, and therefore a model-based approach could not be best suited for this kind of inquire.

Bibliography

[1] Hassan A. et al. "Intelligent Data Engineering and Automated Learning – IDEAL 2013". In: (2013). DOI: 10.1007/978-3-642-41278-3.

[2] Savitzky Abraham and Golay Marcel. "Smoothing and differentition of data by simplified least squares". In: (1964). DOI: 10.1021/ac60214a047.

[3] Allen et al. "Time – frequency analysis of movement-related spectral power in EEG during repetitive movements : A comparison of methods". In: (2010). DOI: 10.1016/j.jneumeth.2009.10.022.

[4] Carlos Amo et al. "Analysis of Gamma-Band Activity from Human EEG Using Empirical Mode Decomposition". In: (2017). DOI: 10.3390/s17050989.

[5] Keith Andrews et al. "Misdiagnosis of the vegetative state: retrospective study in a rehabilitation unit". In: *Bmj* (1996). DOI: 10.1136/bmj.313.7048.13.

[6] A.O. Boudraa, J.C. Cexus, and Z. Saidi. "EMD-Based Signal Noise Reduction". In: *International Journal of Electronics and Communication Engineering* (2004).

[7] Nicolas Brodu, Fabien Lotte, and Anatole Lécuyer. "Comparative study of band-power extraction techniques for Motor Imagery classification". In: *IEEE SSCI 2011 - Symposium Series on Computational Intelligence - CCMB 2011: 2011 IEEE Symposium on Computational Intelligence, Cognitive Algorithms, Mind, and Brain* (2011). DOI: 10.1109/CCMB.2011.5952105.

[8] A. Garcés Correa et al. "Artifact removal from EEG signals using adaptive filters in cascade". In: *Journal of Physics: Conference Series* (2007). DOI: 10.1088/1742-6596/90/1/012081.

[9] Martin Eimer. "The lateralized readiness potential as an on-line measure of central response activation processes". In: *Behavior Research Methods, Instruments, and Computers* (1998). DOI: 10.3758/BF03209424.

[10] Georgios B. Giannakis and Michail K. Tsatsanis. "Signal Detection and Classification Using Matched Filtering and Higher Order Statistics". In: *Acoustics, Speech and Signal ...* (1990).

[11] Ali Hassan et al. "An empirical study to remove noise from single-trial MRCP for movement intention detection". In: *Canadian Conference on Electrical and Computer Engineering* (2015). DOI: 10.1109/CCECE.2015.7129183.

[12] E. Huang et al. “The empirical mode decomposition and the Hilbert spectrum for nonlinear and non-stationary time series analysis”. In: *Proceedings of the Royal Society A: Mathematical, Physical and Engineering Sciences* (1998). DOI: 10.1098/rspa.1998.0193.

[13] Ning Jiang et al. “A brain-computer interface for single-trial detection of gait initiation from movement related cortical potentials”. In: *Clinical Neurophysiology* (2015). DOI: 10.1016/j.clinph.2014.05.003.

[14] Xiaoyan Li, Ping Zhou, and Alexander S. Aruin. “Teager–Kaiser Energy Operation of Surface EMG Improves Muscle Activity Onset Detection”. In: *Annals of Biomedical Engineering* (2007). DOI: 10.1007/s10439-007-9320-z.

[15] Benjamin Libet. “Unconscious cerebral initiative and the role of conscious will in voluntary action”. In: (1985). DOI: 10.1017/S0140525X00044903.

[16] Benjamin Libet et al. “Time of Conscious Intention To Act in Relation To Onset of Cerebral Activity (Readiness-Potential)”. In: (1983). DOI: 10.1093/brain/106.3.623.

[17] Dennis J. McFarland. “The Advantages of the Surface Laplacian in Brain-Computer Interface Research”. In: (2015). DOI: 10.1017/S1092852915000371.Neuroimaging.

[18] Dennis J. McFarland et al. “Spatial filter selection for EEG-based communication”. In: *Electroencephalography and Clinical Neurophysiology* (1997). DOI: 10.1016/S0013-4694(97)00022-2.

[19] Wahiba Mohguen and Raïs El’hadi Bekka. “Improvement of the EMD-SG Denoising Method”. In: *International Journal of Electronics and Electrical Engineering* (2017). DOI: 10.18178.

[20] Imran Khan Niazi et al. “Detection of movement intention from movement-related cortical potentials with different paradigms”. In: *Biosystems and Biorobotics* (2014). DOI: 10.1007/978-3-319-08072-7_42.

[21] G Pfurtscheller and A Aranibar. “Event-Related Cortical Ddesynchronization Detected by Power Measurements of Scalp EEG”. In: (1977).

[22] G. Pfurtscheller and F.H. Lopes da Silva. “Event-related EEG/MEG synchronization and desynchronization : basic principles”. In: *Clinical Neurophysiology* (1999). DOI: 10.1016/S1388-2457(99)00141-8.

[23] G. Pfurtscheller et al. “EEG-based discrimination between imagination of right and left hand movement”. In: *Electroencephaplography and clinical Neurophysiology* (1997).

[24] Gert Pfurtscheller. “Evaluation of Event-Related Desynchronization (ERD) Preceding and Following Voluntary Self-paced Movement”. In: (1979).

[25] Gert Pfurtscheller. “Graphical Display and Statistical Evaluation of Event-Related Desynchronization (ERD)”. In: (1977).

[26] Ahmadian Pouya, Cagnoni Stefano, and Ascari Luca. "How capable is non-invasive EEG data of predicting the next movement? A mini review". In: *Frontiers in Human Neuroscience* (2013). DOI: 10.3389/fnhum.2013.00124.

[27] Hiroshi Shibasaki and Mark Hallett. "What is the Bereitschaftspotential?" In: *Clinical Neurophysiology* (2006). DOI: 10.1016/j.clinph.2006.04.025.

[28] Stanislaw Solnik et al. "Teager–Kaiser Operator improves the accuracy of EMG onset detection independent of signal-to-noise ratio". In: (2008).

[29] Shravani Sur and V. K. Sinha. "Event-related potential: An overview". In: *Industrial Psychiatry Journal* (2009). DOI: 10.4103/0972-6748.57865.

[30] M. Teplan. "Fundamentals of EEG Measurement". In: (2002).

[31] Yang Zhan et al. "Detecting time-dependent coherence between non-stationary electrophysiological signals—A combined statistical and time–frequency approach". In: *Journal of Neuroscience Methods* (2006).